Paleoceanography and Paleoclimatology

RESEARCH ARTICLE
10.1029/2024PA004846

Millennial-Scale Climate Variability Potentially Shaped the Early Interglacial Optimum in Southern Europe

Stéphanie Desprat[1], Gauthier Guillem[1], Maria Fernanda Sánchez Goñi[1], Teresa Rodrigues[2,3], Qiuzhen Yin[4], and Joan O. Grimalt[5]

[1]Environnements et Paléoenvironnements Océaniques et Continentaux (EPOC, UMR 5805), CNRS, Bordeaux INP, EPHE, Université de Bordeaux, PSL University, Pessac, France, [2]Divisão de Geologia e Georecursos Marinhos, Instituto Português do Mar e da Atmosfera, Lisboa, Portugal, [3]Centro de Ciências do Mar (CCMAR), Universidade do Algarve, Faro, Portugal, [4]Earth and Climate Research Center, Earth and Life Institute, Université Catholique de Louvain, Louvain-la-Neuve, Belgium, [5]Institute of Environmental Assessment and Water Research (IDAEA), CSIC, Barcelona, Spain

Abstract The seasonal and latitudinal distribution of insolation is considered the main factor controlling the magnitude and timing of interglacial periods. However, despite small differences in insolation forcing, vegetation and hydrology in southern Europe during past interglacials are variable and the gradual change in insolation cannot explain the observed short-lived forest optimum. Here we focus on vegetation and hydroclimatic changes at orbital- and suborbital-scales in southwestern Europe during two past warm interglacial periods with reduced ice-sheets, namely Marine Isotope Stages (MIS) 9e and 5e. We provide new pollen and sea surface temperatures records for MIS 9e from IODP Site U1385. This pollen record shows a forest expansion in southern Iberia over a 14 ky interval, bracketed by the millennial-scale cooling events of Termination IV and MIS 9d. Between 334.5 and 332.5 ka, forest expansion reached a maximum, suggesting increased winter moisture during early MIS 9e. Model-data comparison for MIS 9e and 5e shows that insolation is the main driver of the orbital-scale vegetation and precipitation changes in Iberia, atmospheric CO_2 forcing playing a secondary role. The high-frequency component of the MIS 9e and 5e forest timeseries highlights the early interglacial forest and precipitation maxima as prominent suborbital events lasting ~2 ky. We propose that the primarily insolation-driven forest and precipitation optima were fostered by the non-equilibrium conditions generated by the millennial-scale deglacial variability during the early interglacials. Additionally, the early end of these optima may have been favored by a cooling and drying event that is part of the persistent intra-interglacial variability.

Key Points:

- MIS 9e pollen and sea surface temperature records from IODP Site U1385 show interglacial climate conditions in southern Europe for 14 ky
- The MIS 9e interglacial, like the MIS 5e one, is marked by millennial-scale intra-interglacial climate variability
- Millennial-scale variability likely played a major in defining the short-lived climate optimum in southern Europe during the MIS 9e and 5e

Supporting Information:

Supporting Information may be found in the online version of this article.

Correspondence to:

S. Desprat,
stephanie.desprat@u-bordeaux.fr

Citation:

Desprat, S., Guillem, G., Sánchez Goñi, M. F., Rodrigues, T., Yin, Q., & Grimalt, J. O. (2024). Millennial-scale climate variability potentially shaped the early interglacial optimum in Southern Europe. *Paleoceanography and Paleoclimatology*, *39*, e2024PA004846. https://doi.org/10.1029/2024PA004846

Received 7 FEB 2024
Accepted 21 AUG 2024

1. Introduction

Two decades of sustained research on interglacial climates have revealed that interglacials of the last 1 million years are, on a global scale, highly diverse in their intensity and duration (Masson-Delmotte et al., 2010; Past Interglacials Working Group of Pages, 2016; Tzedakis, Raynaud, et al., 2009). Furthermore, data compilations and simulations indicate that the magnitude and nature of the climate response during interglacial periods had varied spatially (Lang & Wolff, 2011; Past Interglacials Working Group of Pages, 2016; Yin & Berger, 2015). For instance, the Marine Isotope Stage (MIS) 5e and 9e interglacials are globally recorded as warmer, with particularly pronounced warming at high latitudes, enabling the Greenland ice-sheet to melt substantially (Hatfield et al., 2016; Irvalı et al., 2020). High sea surface temperatures (SST) are also recorded during these interglacials on the Iberian margin (Martrat et al., 2007; Rodrigues et al., 2017). On land, the regional response of the temperature and precipitation to strong global climate warming, as observed during the MIS 10 to 9 and MIS 6 to 5 deglaciations, that is, Terminations II and IV, respectively, still need to be better documented and the forcing factors better understood.

Variations in Earth's orbital parameters, which determine changes in the latitudinal and seasonal distribution of insolation, are pacing deglaciations leading to interglacial periods but cannot alone explain the difference in temperature magnitude between interglacials and the particularly spatially variable hydroclimatic changes (Tzedakis, Raynaud, et al., 2009; Yin & Berger, 2012). Modeling studies have shown that interglacial climate and vegetation on a global scale are mainly driven by the combined forcing of orbital parameters and atmospheric CO_2 but their relative importance would vary from one interglacial to another and across latitudes (Yin & Berger, 2012, 2015). Transient experiments show that the SW Iberian forest dynamics over the MIS 1, 11c, and 19c interglacials were mostly coupled to changes in winter precipitation mainly controlled by precession while

CO_2 played a negligible role (Oliveira et al., 2018). However, a recent study points to atmospheric CO_2 as a major forcing of precipitation and vegetation changes in the eastern Mediterranean region over the past 500 ky, although without clear identification of mechanistic processes (Koutsodendris et al., 2023). We still need to better understand the main factors controlling vegetation and hydrological changes in the Southern European region and how they have shaped them during periods of strong high-latitude warming.

Research on the Iberian margin has been prolific in paleoclimatic sequences, especially deep-sea pollen sequences, which are valuable source of information on vegetation and hydroclimatic changes in southern Europe during past interglacial periods (e.g., Desprat et al., 2007, 2017; Sánchez Goñi et al., 2018; Tzedakis et al., 2004). Pollen records from the SW Iberian margin were used to document the past variations of the warm-temperate forest, also called Mediterranean Forest (MF), mainly formed of temperate deciduous trees and shrubs and sclerophylls. These records show a particularly strong expansion of the MF, suggesting increased temperatures and winter precipitation during the first millennia of the most recent interglacial periods MIS 9e, MIS 7e (Tzedakis et al., 2004), MIS 5e (Sánchez Goñi et al., 1999; Tzedakis et al., 2018) or MIS 1 (Chabaud et al., 2014; Oliveira et al., 2018). However, the gradual change in orbital forcings over the course of these interglacials cannot explain this regional short-lived optimum in forest and humid conditions. Based on the apparent co-variation of forest extent and atmospheric CH_4 concentrations during MIS 9e and 7e, a control of the position of the Intertropical Convergence Zone (ITCZ) on the relative influence of the mid-latitude and tropical atmospheric circulations has been proposed to explain the strong seasonal supply in moisture to southern Iberia during the early intervals of interglacials (Tzedakis, Pälike, et al., 2009). However, the MIS 9e record from core MD01-2443 in the SW Iberian margin remains puzzling. It shows that the MF developed in the southwestern Iberian Peninsula for only 3.6 ky at the beginning of the MIS 9e (Tzedakis et al., 2004), whereas in the northwest of the peninsula, the temperate forests, mainly composed of deciduous elements, thrived for a much longer period of 12 ky, during most of MIS 9e (Desprat et al., 2009). In addition, no collapse of the MF is observed during other interglacials in southern Iberia. Only one speleothem record from the southern Balkans shows wet conditions during MIS 9e for only 5 ky (Regattieri et al., 2018) although the timing appears to be different from the wet period in the SW Iberia. The reason of this early forest collapse in southern Iberia remains enigmatic, as it occurs without any change in ice volume or sea surface temperature (Tzedakis et al., 2004). The authors suggested that it could be the result of a millennial-scale event, albeit undetected in the marine proxy records of the same core.

There is growing evidence that millennial-scale variability persisted through the last 1.5 Myr, even during past interglacial periods, albeit generally with lower amplitudes than during glacial periods or glacial inceptions due to the weak or absence of amplification by ice feedbacks (McManus et al., 1999; Past Interglacials Working Group of Pages, 2016; Sun et al., 2021). In southern Europe, repeated drying and cooling events have been recorded during the last interglacial (Tzedakis et al., 2018), and the MIS 11c and MIS 19c interglacials (Kousis et al., 2018; Oliveira et al., 2016; Sánchez Goñi et al., 2016; Sassoon et al., 2023), but the resolution of the available records does not allow yet to resolve millennial to centennial variability during MIS 9e. It is also becoming increasingly clear that abrupt climatic changes on millennial time scales (10^3–10^4 years) are not only superimposed on the climatic variations occurring on orbital timescales (10^4–10^6 years) but that the two variabilities, millennial and orbital, interact. For instance, after the Mid-Pleistocene Transition, in complement to glacial amplification, the magnitude of millennial-scale climate variations from high- to low- latitudes appears to be modulated by the orbital forcing (Sánchez Goñi et al., 2008; Sun et al., 2021; Zorzi et al., 2022). The reverse is also true, with millennial-scale variability amplifying orbital forcing, explaining for instance the substantial accumulation of ice from MIS 5a to MIS 4 at around 70 ka (Sánchez Goñi et al., 2013). As recently proposed, the terminal millennial-scale events of the deglaciations, marked by a dramatic reduction in the AMOC and massive iceberg discharges in the North Atlantic may have altered the climate response to orbital forcing during the early millennia of the interglacial periods in generating non equilibrium conditions (Barker et al., 2019; Barker & Knorr, 2021; Deaney et al., 2017). The influence of millennial-scale variability on orbital-scale climate response is less commonly proposed but has strong implications for defining the climate optimum of an interglacial period and its intensity, and the contribution of controlling factors (Barker et al., 2019).

Here we present a new high-resolution pollen record from the IODP Site U1385, collected on the SW Iberian margin, spanning the MIS 9e interglacial. In this study, a comparison of the MIS 9e records with published MIS 5e records from the Iberian margin is proposed to characterize the orbital-scale response of vegetation and hydroclimate in southwestern Europe during past warm interglacials and a model-data comparison will be presented to estimate the relative contribution of the CO_2 and insolation forcing on these changes. In addition, the

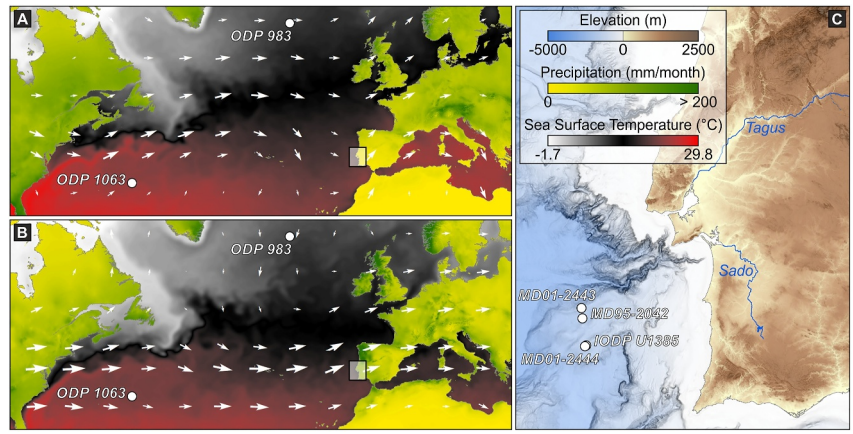

Figure 1. Site location and physiographic elements of the North Atlantic region. Left panels: maps representing the (a) summer and (b) winter sea surface temperatures (°C), winds (arrows) and precipitation over land (mm) as well as sites mentioned in the text. The IODP Site U1385 (this study) and previously published pollen records from the southwestern Iberian margin are located on the map of the right panel. Colors on this map represent the bathymetry of the margin and the relief of the peninsula.

intra-interglacial variability during MIS 9e and 5e is investigated using timeseries analyses allowing to extract the high-frequency component of forest pollen timeseries. We will focus most particularly on the potential influence of this variability in shaping the forest and moisture optimum of the interglacials. We selected the MIS 9e and 5e interglacials because the residual Northern Hemisphere ice-sheets were particularly small due to significant warming at high latitudes but related to different insolation and greenhouse gas forcings. While MIS 5e is marked by a greater insolation forcing during boreal summer, MIS 9e exhibits stronger GHG forcing at minima in precession (P_{min}).

2. Materials and Methods

2.1. The Site U1385 and Modern Physio- and Phyto-Geographic Context

The investigated IODP site U1385 was recovered during IODP Expedition 339 on a spur on the continental slope of the southwestern Iberian margin (37°34.285′N, 10°7.562′W, 2578 m.b.s.l.) at 2,656 m water depth, off the mouth of the Tagus River (Figure 1). It is in close proximity to the extensively studied Marion Dufresne piston cores MD95-2042, MD01-2444 and MD01-2443. The latter is only 26 km away from Site U1385. Detailed information on the drilling procedure and sedimentation at Site U1385 can be found in Hodell, Crowhurst, et al. (2013) and Hodell, Lourens, et al. (2013).

At present, the main upper water masses above Site U1385 are the different modes of the Eastern North Atlantic Central Water conveyed by the Portuguese Current System (Pérez et al., 2001). SST for the site area are ∼16°C in winter and ∼20°C in summer (Salgueiro et al., 2008). At depth, the site is under the influence of the Northeast Atlantic Deep Water (NEADW). Information on the modern deep and surface hydrography above the site is detailed in previous publications (e.g., Rodrigues et al., 2017; Sánchez Goñi et al., 2016).

IODP Site U1385 mainly recruits pollen from the Mediterranean vegetation that dominates the major river basins of southwestern Iberia (i.e., the Tajo and Sado rivers), as shown in a previous study of surface pollen samples from the southwestern Iberian margin (Naughton et al., 2007) and the comparison between present-day pollen assemblages from the vegetation of the Tagus basin and marine and estuarine pollen assemblages from the sea-sediment surface representing the last centuries (Morales-Molino et al., 2020). The composition of the Mediterranean vegetation varies according to the altitude and the continentality (Blanco Castro et al., 1997). At lower altitudes, the oleo-lentisc formation is found in the warmest areas. Otherwise, evergreen oak woodlands (*Quercus rotundifolia*, *Q. suber*) dominate, with evergreen shrubs such as pistachio (*Pistacia terebinthus*), phillyrea (*Phyllirea angustifolia*), and rockrose (*Cistus*). As the maritime influence decreases eastward, the evergreen oaks are associated with juniper (*Juniper communis*) and Aleppo pine (*Pinus halepensis*). In the mountain ranges, due to the increase in rainfall and the decrease in temperature promoted by the altitudinal gradient, deciduous oak

woods (*Quercus pyrenaica*, *Q. faginea*) dominate the mid-altitude landscapes, while pine woods (*Pinus sylvestris*, *P. nigra*) with juniper develop at higher altitudes. In humid mountainous areas, we can also find heather (Ericaceae). This vegetation thrives in the Mediterranean climate, which is highly seasonal, with wet, mild winters and hot, dry summers (Peinado Lorca & Martínez-Parras, 1987). Winter moisture is brought to Iberia by the prevailing westerly winds, which intensity and direction are currently controlled by the North Atlantic Oscillation (Trigo et al., 2004). Dryness in summer is induced by the development of the Azores anticyclone in the North Atlantic subtropics, which is related to the seasonal migration of atmospheric cells.

2.2. The Proxy Records: Vegetation and SST Reconstructions From Site U1385

Past vegetation changes in SW Iberia and offshore SST are documented in this study using pollen and Uk'_{37}-SST analyses of sediments from the IODP Site U1385 over the interval 47.46 and 43.96 crmcd (corrected revised meter composite depth). Sediment from Holes D and E was subsampled at intervals of 3–16 cm for pollen analysis with increased resolution (3–4 cm) over the interval 46–45.15 m crmcd and every 2 cm for biomarker analysis.

The pollen sample preparation protocol is briefly described below; more details can be found on the webpage of the EPOC laboratory (https://www.epoc.u-bordeaux.fr/index.php?lang=fr&page=eq_paleo_pollens). Sediment samples were first washed and sieved at 150 µm. *Lycopodium* marker grains (exotics) were added to each sample prior to chemical treatments to determine pollen concentrations. Successive chemical treatments were applied to the sediment fraction lower than 150 µm (cold HCl at 10%, at 25% and 50%, cold HF at 45% and at 70%, cold HCl at 25%). After sieving through a 10 µm nylon mesh screen, the residue was mounted in glycerol without staining. Pollen grains were counted using a light microscope at 400X and 1,000X (oil immersion) magnifications. Three out of the 60 samples analyzed were considered sterile due to low pollen concentration. Pollen percentages for each taxon were calculated from a main pollen sum which excluded pollen of *Pinus* and aquatic plants, pteridophyte spores, and indeterminable and unknown pollen. *Pinus* percentages were estimated from the main sum plus *Pinus*. We excluded *Pinus* from the main sum because of it is overrepresentated in marine sediments due to high production rates and high buoyancy in air and water (Heusser & Balsam, 1977; Turon, 1984). Percentages of indeterminable and unknown pollen, spores, and aquatic pollen were calculated from the total pollen and spore sum.

New biomarker analyses were performed to extend the U1385 Uk'_{37}-SST record from Rodrigues et al. (2017) to MIS 9c. Detailed information on the procedure is given in Rodrigues et al. (2017).

2.3. Data Analysis

To decompose the time series into low-frequency and high-frequency signals, we performed, as in Tzedakis et al. (2018), a Gaussian smoothing of the MF, sclerophylls and Ericaceae percentages as well as benthic $\delta^{13}C$ from Site U1385. For that, we used the R package *smoother* (Hamilton, 2015). The bandwidth for the kernel smoothing was chosen to provide smoothing over a window of 7 ky. Such a window is commonly used in the literature to separate the millennial-scale variability of a time series from the changes attributable to orbital forcing (Barker et al., 2011, 2019). The high-frequency component was obtained by calculating the residuals between the unsmoothed original data and the smoothed time series. We performed a final Gaussian smoothing with a bandwidth of 0.7 ky to reduce noise as recommended by Barker et al. (2011). Prior to data processing, we interpolated the original data to obtain evenly spaced time series, which is an essential step for applying a regular smoothing window. The steps chosen depend on the original time resolution of the series. To avoid oversampling or underrepresentation of the high-frequency changes, we selected a constant step of 0.3 ky.

Since the choice of filtering method is known to be mostly arbitrary, we used different methods on the MF time series with variable interpolation steps (from 0.1 to 1.3 ky) and smoothing windows (from 5 to 10 ky) to estimate the global envelopes of the filters (orbital component) and residuals (millennial component) and to test whether the choice of smoothing method, window and interpolation affects the results (Figures S1–S3 in Supporting Information S1). In addition to Gaussian smoothing, we performed a moving average smoothing (method used in Barker et al., 2011, 2019) using the R package *stats*. We also performed a locally weighted regression smoothing (using the R package *stats*) that unlike moving average but like Gaussian smoothing, handles the boundaries We also used a Taner low-pass filter performed using the R package *astrochron*. We calculated the global envelope of the low-pass filtered signal and of the residuals from the results obtained with the different smoothing procedures, windows and interpolation steps, using the R package GET (Myllymäki & Mrkvička, 2023). Note that all

residuals obtained with different smoothing methods show similar main features (Figure S1 in Supporting Information S1). Therefore, we used the 7 ky Gaussian filter as the orbital component and the corresponding residuals as the millennial-scale component of the timeseries. Finally, as in Barker et al. (2011, 2019) and Tzedakis et al. (2018), we applied a final high-pass filter to the residuals to reduce noise. We chose a Gaussian filter and applied a cutoff frequency of 1/700 years^{-1}, which has been shown to be a reasonable compromise between noise reduction and signal fidelity (Barker et al., 2011).

We also estimated rates of vegetation change during MIS 9e. The dissimilarity matrix was calculated from the pollen assemblage percentages using Bray-Curtis dissimilarity (Anderson et al., 2022) and square chord distance (Overpeck et al., 1985) using the R package *vegan* (Oksanen et al., 2022). These metrics allow a quantification of the difference between two adjacent pollen samples. The rate of change (RoC) corresponds to the ratio between dissimilarity and age difference between two consecutive samples.

2.4. LOVECLIM Simulations

Climate and vegetation simulations were performed using the EMIC model LOVECLIM. A detailed description of the model and experimental design used in this study can be found in Yin and Berger (2012, 2015). Here, we present the results of the snapshot experiments representing the MIS 9e and MIS 5e interglacial peaks. These experiments use the following setting: astronomical parameters fixed at the $\delta^{18}O$ peak dates (123 and 329 ka) in the LR04 stack, greenhouse gas (GHG) concentrations at the time of the interglacial CO_2 peaks (Lüthi et al., 2008), and ice-sheets in their current configuration. Anomalies in tree fraction (%), annual, JJA, and DJF precipitation (cm.year^{-1}) and annual, JJA, and DJF temperature (°C) between MIS 5e and MIS 9e were calculated.

2.5. Chronological Framework

For the interval between 47.46 and 45.98 crmcd, we used the chronology provided by Nehrbass-Ahles et al. (2020), which is based on the synchronization of IODP Site U1385 with EDC on the AICC2012 age scale based on the alignment of the benthic $\delta^{18}O$ and δD records. For the upper part between 45.98 and 43.79 crmcd, we used the Greenland synthetic age model established for Site U1385 by Hodell et al. (2015), but transferred it to the AICC2012 chronology using the Greenland synthetic temperature (GL_T_syn) record from Barker et al. (2019). All records for the MIS 9e interval from the piston cores MD01-2443 and MD01-2444 are shown on the GL_T_syn age provided by Hodell, Crowhurst, et al. (2013) and Hodell, Lourens, et al. (2013) that we also transferred to the AICC2012 chronology.

3. Results From Site U1385 Pollen and SST Records

The pollen record from IODP Site U1385 (Figure 2, Figure S4 in Supporting Information S1) suggests a shift in vegetation during Termination IV. At ∼334.5 ka, glacial semi-desert plants (mainly *Artemisia* and Amaranthaceae) with scattered pine and juniper woodlands were abruptly replaced by temperate deciduous trees and shrubs and the sclerophylls (mainly *Quercus* evergreen and *Olea*), forming the MF also called warm-temperate forest. Concurrently, the Site U1385 record show an abrupt deglacial SST warming of 11°C, abrupt increases in benthic $\delta^{13}C$ and Ca/Ti ratio and a decrease in Zr/Si values (Figure 2). The planktic $\delta^{18}O$ record shows progressively decreasing values between 343 and 335 ka. Both the MF percentages and SSTs reach MIS 9e maximum values between 334.5 and 333 ka (56%, 21°C, respectively). Pollen data show a short-lived MF optimum, ending at ∼333 ka, while SSTs remained above 20°C until 327.9 ka. However, the MF and in particular the sclerophylls (i.e., the Mediterranean taxa s.s.) remain on average higher until the end of the SST optimum than in the remaining part of MIS 9e. While SSTs gradually decreased after 327.9 ka, sclerophylls declined in favor of semi-desert taxa. At ∼320.5 ka, that is, 3–4 millennia after the end of MIS 9e, the U1385 records display a reduction in temperate trees well below 20% in favor of semi-desert plants along with a 4°C SST cooling, a strong decrease in Ca/Ti ratio, a marked increase in Zr/Sr ratio and planktic $\delta^{18}O$ and lower values in benthic $\delta^{13}C$. After a brief increase in forest and SST, Site U1385 records show a second episode of forest and SST reduction of lesser intensity at ∼315 ka, before a new expansion of MF.

During the forest interval between 334.5 and 320.5 ka, the MF mostly oscillates between 20% and 30%, with several brief drops below 20%. Over the first millennia of MIS 9e, these drops are clearly marked by a reduction in Mediterranean trees and shrubs in favor of Ericaceae which becomes an important element of the evergreen shrublands. Although heath species can bear summer dryness, soil humidity/annual rainfall must be sufficient and

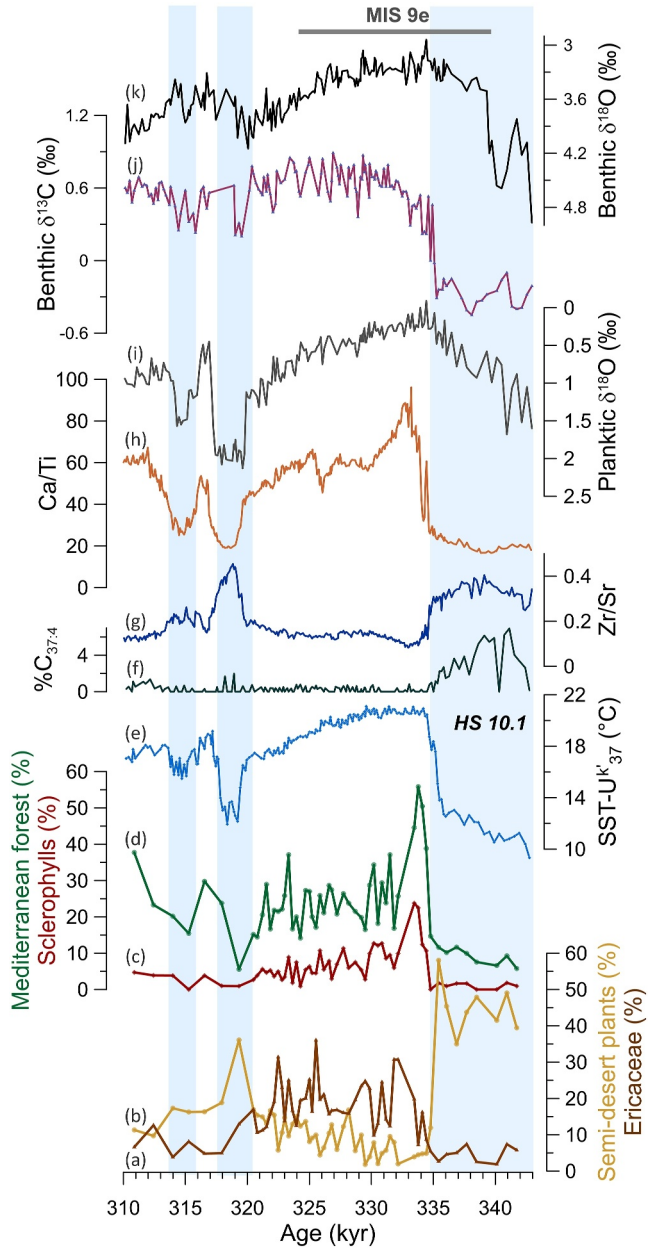

Figure 2. Multi-proxy record from IODP Site U1385 across MIS 9e. From the bottom to the top: Percentages of major pollen taxa or ecological groups (this study): (a) Ericaceae, (b) Semi-desert plants (Amaranthaceae, *Artemisia*, *Ephedra fragilis*-type et *Ephedra distachya*-type), (c) Sclerophylls (mainly evergreen *Quercus* type, *Quercus suber* type, *Cistus*, *Olea*, *Phillyrea*, *Pistacia*), (d) Mediterranean forest including all warm temperate trees and shrubs (are not included the pioneer elements *Betula*, Cupressaceae and *Hippophäe* and the cool temperate trees *Abies* and *Fagus*); (e and f) sea surface temperature estimations from Uk'_{37} (this study) and percentages of $C3_{7:4}$ (this study) used as indicator of cold events associated with iceberg discharges (Rodrigues et al., 2017); (g and h) XRF data: Ca/Ti and Zr/Si (Hodell et al., 2023b); (i and j) Planktic $\delta^{18}O$ measured on *Globigerina bulloides* and benthic $\delta^{13}C$ measured on *Cibicidoides wuellerstorfi*, data are from Nehrbass-Ahles et al. (2020) between 343 and 329 ka and from Hodell et al. (2023b) down to 329 ka; and (k) benthic $\delta^{18}O$ from mixed species corrected to *Uvigerina peregrina* (Hodell et al., 2023b).

a year-round distribution of the rainfall appears preferential (Loidi et al., 2007, 2010) while Mediterranean plants thrive in areas with warm and dry summer season. The repeated declines in sclerophylls to the benefit of heathland suggest therefore shifts in the seasonal distribution of precipitation with decreased winter precipitation and increased summer ones and likely a decrease in temperature.

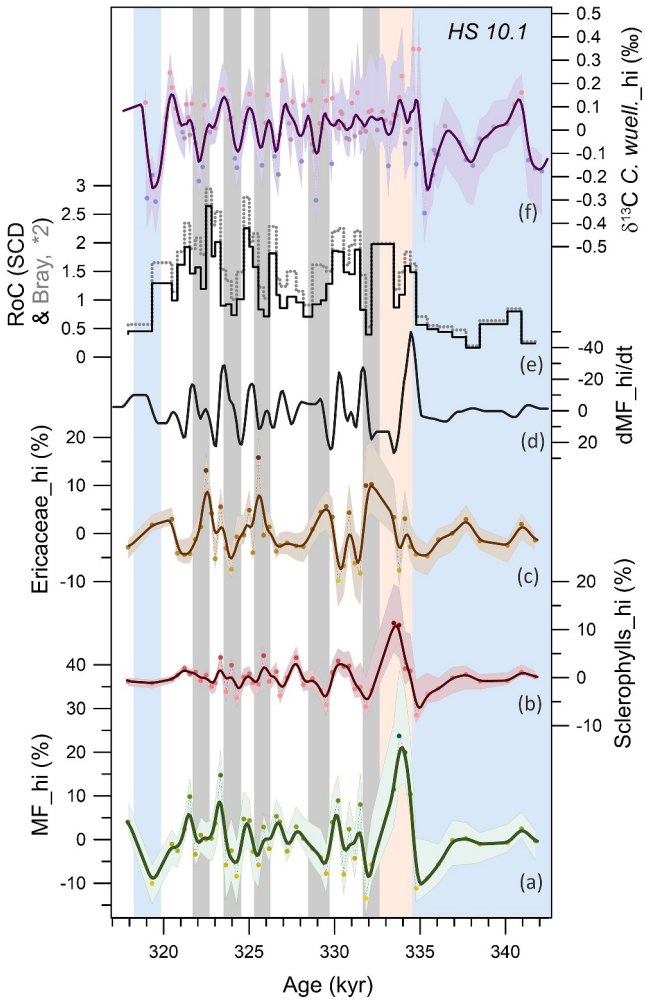

Figure 3. Millennial-scale changes in the pollen and benthic $\delta^{13}C$ records from IODP Site U1385. From the bottom to the top: (a–c) high-frequency component of the Mediterranean forest pollen (MF_hi), sclerophylls and Ericaceae percentages (dashed dotted lines: residuals of the 7 ky-Gaussian smoothing, thick line: residuals smoothed with a 0.7 ky-Gaussian filter, colored area: global envelope), (d) dMF_hi/dt: rate of change (RoC) of the MF_hi signal using the smoothed residuals, (e) Step plot of the rate of change of the pollen assemblages based on Bray-Curtis distance (dotted line) and squared Chord distance (bold line), (f) U1385 benthic $\delta^{13}C$_hi: high frequency component of the *C. wuellerstorfi* $\delta^{13}C$ (Hodell et al., 2023b; Nehrbass-Ahles et al., 2020) (dashed dotted lines: residuals of the 7 ky-Gaussian smoothing, thick line: residuals smoothed with a 0.7 ky-Gaussian filter, colored area: global envelope). Blue bands correspond to the cold millennial-scale events of the deglaciation (HS 10.1) and of MIS 9d. Pink band indicates the suborbital anomalous warm and humid event at the beginning of MIS 9e and the gray bands, the millennial-scale intra-interglacial cooling and drying events in Iberia.

The high frequency component of the MF time series (MF_hi) highlights the brief peak in forest at the beginning of MIS 9e and a series of suborbital decreases in forest detected at ~332, 329, 326, 324, and 322 ka (Figure 3). These short episodes are also evidenced by abrupt variations in the RoC of the MF. Calculation of the RoC from the pollen assemblages shows clear abrupt and repeated shifts of the ecosystems during the interglacial period of MIS 9e. Using the squared chord distance or the Bray-Curtis coefficient does not change the results. With the exception of around 333 ka, where the increase in RoC may be an artifact of the large interval between two samples, the variations in RoC during the interglacial are not caused by changes in sampling resolution which is nearly constant over this interval (Figure S5 in Supporting Information S1). These episodic reductions in MF are clearly marked in the sclerophyll percentages at the beginning of MIS 9e (Figure 2). This pattern of palynological turnover suggests that short-term vegetation changes are the result of suborbital cooling and drying episodes in southwestern Europe. As these episodes are characterized by a recurrence between 1.5 and 2.5 ky, we will refer to them hereafter as millennial-scale episodes although intra-interglacial variability is often referred to as multi-centennial scale variability.

4. Discussion

4.1. Duration of the Forest Stage During the MIS 9e Interglacial in SW Iberia

Because of the long history and strong heritage of palynology in continental interglacial studies, the distinction between forest interval and interglacial period has long been tenuous. Palynologists used to define interglacial periods in northwestern Europe from pollen records as successive biostratigraphic units characterized by pollen assemblages describing a forest stage (Turner & West, 1968). From continental records, the lower limit of a forest stage has classically been defined on the basis of biostratigraphic criteria corresponding to the point in a pollen diagram where arboreal pollen exceeds 50% of the pollen sum at the beginning of an interglacial forest succession (Turner, 2002). Because the pollen source area is larger for marine sites, possibly integrating various environments with abundant herbaceous communities, Tzedakis et al. (2004) lowered the arboreal pollen threshold to 20% to define the limits of forest stages (including those of MIS 9e) in the core MD01-2443. The use of such a threshold resulted in the delineation of a very short forest stage of 3.6 ky-long, leading these authors to speak of a short-lived interglacial during MIS 9e. The new high-resolution pollen record from Site U1385 also shows a brief maximum of MF forest expansion in early MIS 9e (Figure 4), which, as in core MD01-2443, coincides with the peak in Ca/Ti values (Hodell, Crowhurst, et al., 2013). However, in Site U1385, the slightly higher overall proportion of arboreal pollen and higher time resolution cause the arboreal pollen curve to repeatedly reach values above 20% invalidating the atypically short duration of the forest stage in SW Iberia during MIS 9e. Threshold values should be used with caution, as we can see here that a non-significant/small difference can lead to a different interpretation. The pollen record from Site U1385 shows a forested interval in SW Iberia during MIS 9e that is similar in length to that observed in core MD03-2697 in northwestern Iberia (Desprat et al., 2009). Although the individual chronologies of the terrestrial pollen records and their uncertainties preclude detailed comparison, the Praclaux pollen sequence in southern France (Reille & de Beaulieu, 1995; Tzedakis et al., 2001) and the Lake Ohrid and Tenaghi Philippon sequences in Greece (Koutsodendris et al., 2023; Sadori et al., 2016; Tzedakis et al., 2006; Wagner et al., 2019) also suggest a substantial amount of forest during the MIS 9e lasting more than ten thousand years. Such a period of dominant forest landscape recorded in the southern

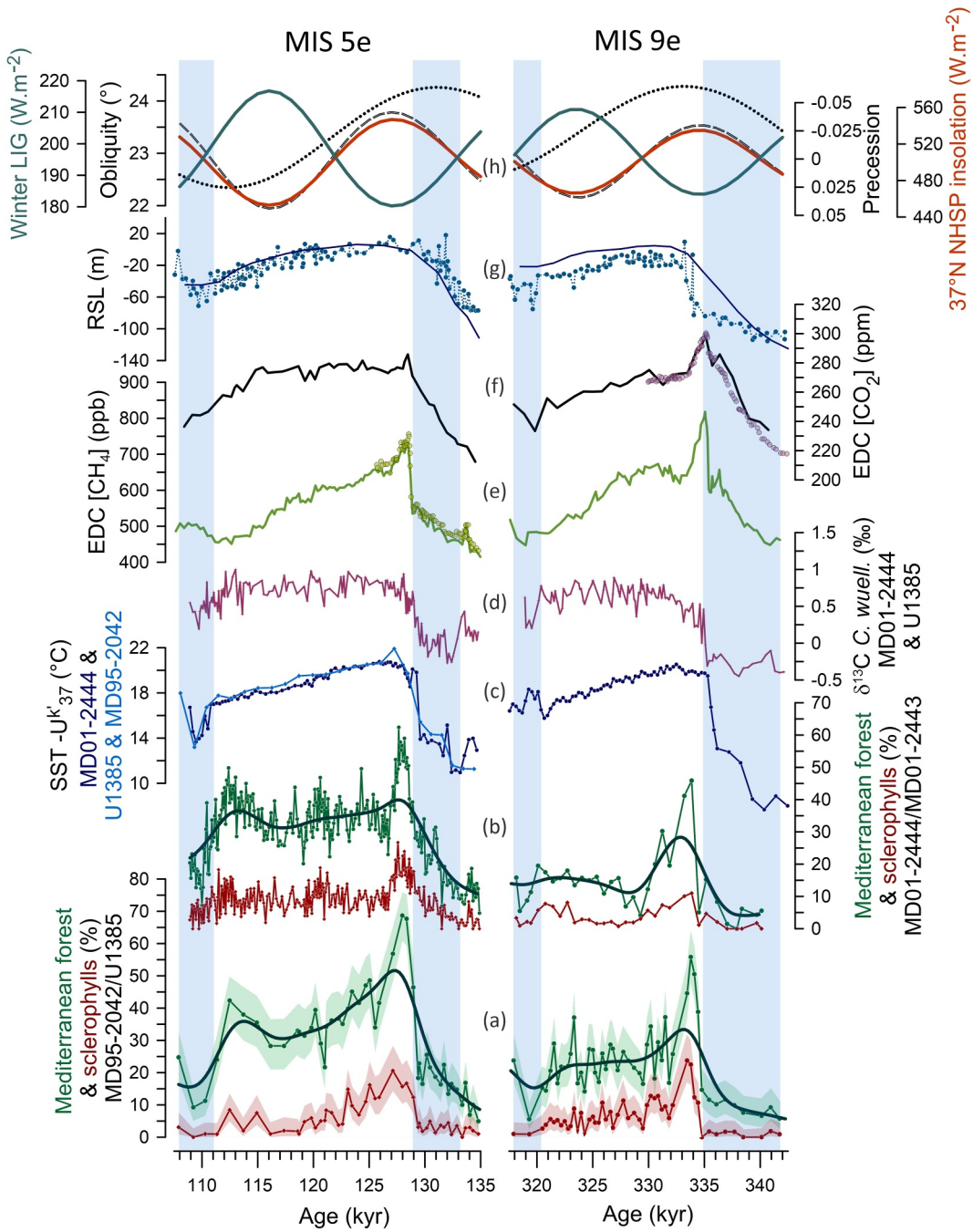

Figure 4. Orbital-scale variability during MIS 9e and MIS 5e in the southwestern Iberian margin records and forcing factors. From bottom to top: Mediterranean forest (green dots) and taxa (red diamonds) percentages for MIS 9e and 5e (a) from sites U1385 (this study) and MD95-2042 (Sánchez Goñi et al., 1999) and (b) from sites MD01-2443 (Tzedakis et al., 2004) and MD01-2444 (Tzedakis et al., 2018), with shading areas indicating 95% confidence interval on pollen percentages calculated using the R package *binom* (Dorai-Raj, 2022) and bold lines representing the orbital component of the timeseries obtained using a 7 ky-Gaussian smoothing filter; (c) SST-Uk'$_{37}$ from Site U1385 (MIS 9e, this study), MD95-2042 (MIS 5e, Pailler & Bard, 2002) in sky blue (diamonds) and from core MD01-2444 (Hodell, Crowhurst, et al., 2013; Tzedakis et al., 2018) in dark blue (circles); (d) δ^{13}C measured on *C. wuellerstorfi* from Site U1385 (Hodell et al., 2023b; Nehrbass-Ahles et al., 2020) and MD01-2444 (Tzedakis et al., 2018); (e) Atmospheric CH_4 concentrations from EPICA-Dome C ice core on the AICC2012 chronology (Bazin et al., 2013; Nehrbass-Ahles et al., 2020), dots represent the high resolution data from Schmidely et al. (2021); (f) Atmospheric CO_2 concentrations from EPICA-Dome C ice core on the AICC2012 chronology (Bereiter et al., 2015), dots represent the high resolution data from Nehrbass-Ahles et al. (2020); (g) Relative sea-level from Waelbroeck et al. (2002) (thick lines) and Rohling et al. (2019) and Grant et al. (2012) (dotted lines), (h) Orbital parameter and local summer insolation and latitudinal insolation gradient between 60°N and 30°N when northern hemisphere summer is at perihelion (NHSP) and when northern hemisphere winter is at aphelion (NHWA) using insolation calculation from Berger and Loutre (1991). MIS 5 data are shown on their original chronology. All MIS 9e data from Site U1385, core MD01-2443 and MD01-2444 are on the AICC2012 chronology (cf., Section 2).

European sequences defines the regional interglacial, that is, the interval with the peak interglacial climate that lasted ∼14 ky in this region on the AICC2012 chronology.

Moving away from pollen-based biostratigraphy, which can face the inherent problems of both defining boundaries from pollen percentages and geographical variations in ecosystem response that define regional interglacial climates, the most comprehensive definition of an interglacial period, originally related to continental ice-sheet size, was given by the Past Interglacial Working Group (2016). It states that interglacial periods are end-members of glacial cycles characterized by a strongly reduced extent of continental polar ice, caused by globally warm conditions in between the deglaciation and glacial inception. Marine isotope stratigraphy has largely been used to delineate interglacial periods, as $\delta^{18}O$ of deep sea-water provides information on ice volume variations, although this proxy is affected by several biases, including deep-water temperature and hydrographic effects of variable influence through time (Past Interglacials Working Group of Pages, 2016).

It has been clearly demonstrated that the interval of interglacial climate in a region does not strictly coincide with the interval of light benthic $\delta^{18}O$ values that define the interglacial isotopic period at a global scale. Using the MD95-2042 sequence from the Iberian margin, Shackleton et al. (2003) showed that the boundaries of MIS 5e and the Eemian interglacial are different. The same is observed for the period of reduced global ice volume defining MIS 9e and the interval of interglacial climatic conditions that allowed forest expansion in southern Europe and warm SSTs at the Iberian margin. At Site U1385, this interval is bracketed by two major millennial-scale events, recorded between 344–334.5 ka and 320.5–313.5 ka, characterized by low values in Ca/Ti ratio and the dominance of semi-desert plants (Figure 2). Concomitant strong increases in Zr/Si ratio and benthic $\delta^{13}C$ and reduction in SST attest to abrupt cooling and reduction of the North Atlantic oceanic circulation during the MIS 10-9e deglacial transition (TIV) and at the end of MIS 9d (Hodell et al., 2015, 2023a; Nehrbass-Ahles et al., 2020). Coeval high-latitude cooling and ice-rafting episodes, the first of which is referred to as the HS10.1 event, have been documented from the northern North Atlantic sediments (Barker et al., 2019; Mokeddem & McManus, 2017). As previously observed for MIS 5e, and according to Broecker & van Donk (1970), MIS 9e begins at the mid-point of the Termination IV which is dated at ∼340 ka at the latest (on the AICC 2012 chronology), whereas interglacial climatic conditions in southern Europe actually begin at ∼335 ka, when the terminal millennial event of TIV ended. Conversely, MIS 9e terminated 3 to 4 millennia before the forest collapse and abrupt SST decrease associated with the North Atlantic iceberg discharges that identify the millennial event marking the reactivation of the bipolar see-saw during MIS 9d. Therefore, our results indicate that the southern European interglacial climate and the MIS 9e interglacial period both lasted for at least 14 ky, in contrast to the previously proposed short duration (3.6–5 ky) of this interglacial based on regional records (Regattieri et al., 2018; Roucoux et al., 2006; Tzedakis et al., 2004). According to Tzedakis et al. (2012), interglacial periods are bounded by millennial-scale variability, which implies activation of the bipolar see-saw and ice-sheets large enough to fragment. However, based on MIS 5e sea-level changes, they proposed that the substantial accumulation of polar ice in the northern hemisphere that demarcates the end of an interglacial, would occur at least 3 ky before the abrupt post-interglacial cooling event and in the case of MIS 5 and 9, after the end of MIS 5e and MIS 9e. Following this line of reasoning, the interglacial climates that allow minimum ice volume conditions at the northern high latitudes would last for 11 ky during MIS 9e.

4.2. Orbital-Scale Changes in Vegetation and Climate in Southern Europe During Interglacials With Strong High Latitudes Warming: The MIS 5e and MIS 9e Interglacials

4.2.1. A Common Interglacial Evolution

Pollen records from Site U1385 and core MD01-2443 both support a major expansion of MF in the south of the Iberian Peninsula during the first millennia of the MIS 9e interglacial. The orbital component of the MF time series (Gaussian smoothed data, MF_orb) displays maxima close to when the Earth's orbital configuration was at Pmin (Figure 4). This suggests that a moisture optimum, resulting from intensified winter precipitation, was reached in Pmin situation, shortly after the end of the abrupt deglaciation event (HS 10.1). As shown by pollen records from the southern Iberian margin, such an optimum of winter precipitation in southern Europe at Pmin is a feature common to other interglacials such as MIS 5e (Figure 4, Sánchez Goñi et al., 1999; Tzedakis et al., 2018), as well as MIS 7e and the Holocene (Chabaud et al., 2014; Sánchez Goñi et al., 2018; Tzedakis, Pälike, et al., 2009). Enhanced winter precipitation during past interglacial periods is also indicated by long continental pollen records from the north-central Mediterranean such as Lake Ohrid (Wagner et al., 2019). Both

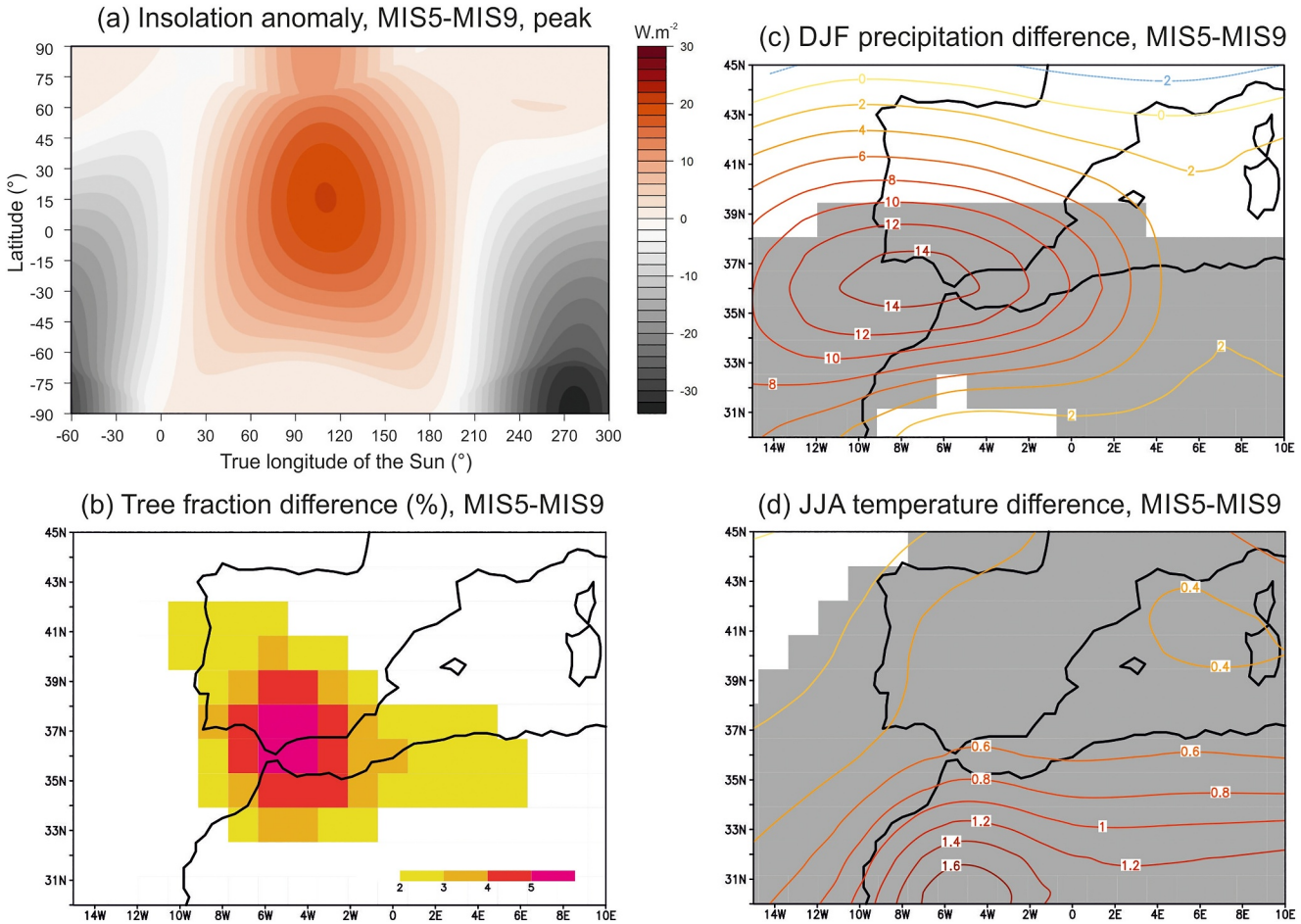

Figure 5. Simulated anomaly in vegetation and climate between MIS 5e and MIS 9e in the Iberian Peninsula. (a) Anomaly in latitudinal and seasonal insolation between 123 and 329 ka, corresponding to the dates chosen as the interglacial peaks of MIS 5e and MIS 9e in Yin and Berger (2012, 2015). Simulated differences in (b) tree fraction in %, (c) December-January-February (DJF) precipitation in cm·year^{-1}, and (d) June-July-August (JJA) temperature in °C between MIS5e and MIS 9e issued from the peak interglacial simulations from Yin and Berger (2012, 2015).

the MD01-2444/MD01-2443 record and the MD95-2042/U1385 record show that the MIS 5e and MIS 9e forest maxima are partly the result of a large expansion of Mediterranean trees and shrubs, such as evergreen oaks, olives, and pistachios, suggesting increased summer aridity and warm temperatures. The strong seasonality of precipitation in southern Europe that characterizes the first millennia of interglacial periods, is most often attributed primarily to the seasonal forcing of insolation (Figure 4). In summer, the precession-induced insolation maximum in the Northern Hemisphere favors summer drought through the strengthening of subtropical anticyclones and the northward migration of the ITCZ. In winter, insolation reaches a minimum in the Northern Hemisphere when the Earth is at aphelion, leading to a southward migration of atmospheric convection cells. Southern Europe then comes under the influence of the moisture-laden westerlies. Davis and Brewer (2009) and Wagner et al. (2019) suggested that the seasonal latitudinal insolation gradient (LIG) is an additional factor that enhances winter precipitation in southern Europe in the early part of interglacial periods. As the winter insolation in the northern hemisphere is reduced more strongly in tropical and subtropical latitudes than in the high latitudes at Pmin, the winter LIG is smaller and the westerlies weaken and shift southward, enhancing precipitation in southern Europe (Kutzbach et al., 2014). Over the course of the MIS 9e and 5e interglacials, although less obvious in the MF_orb component from the MD01-2443/MD01-2444 record, the MF and especially the sclerophyll elements decrease, showing a Mediterranean climate attenuation, while insolation and LIG increase at NHWA (Northern Hemisphere Winter Aphelion) and decrease at NHSP (Northern Hemisphere Summer Perihelion).

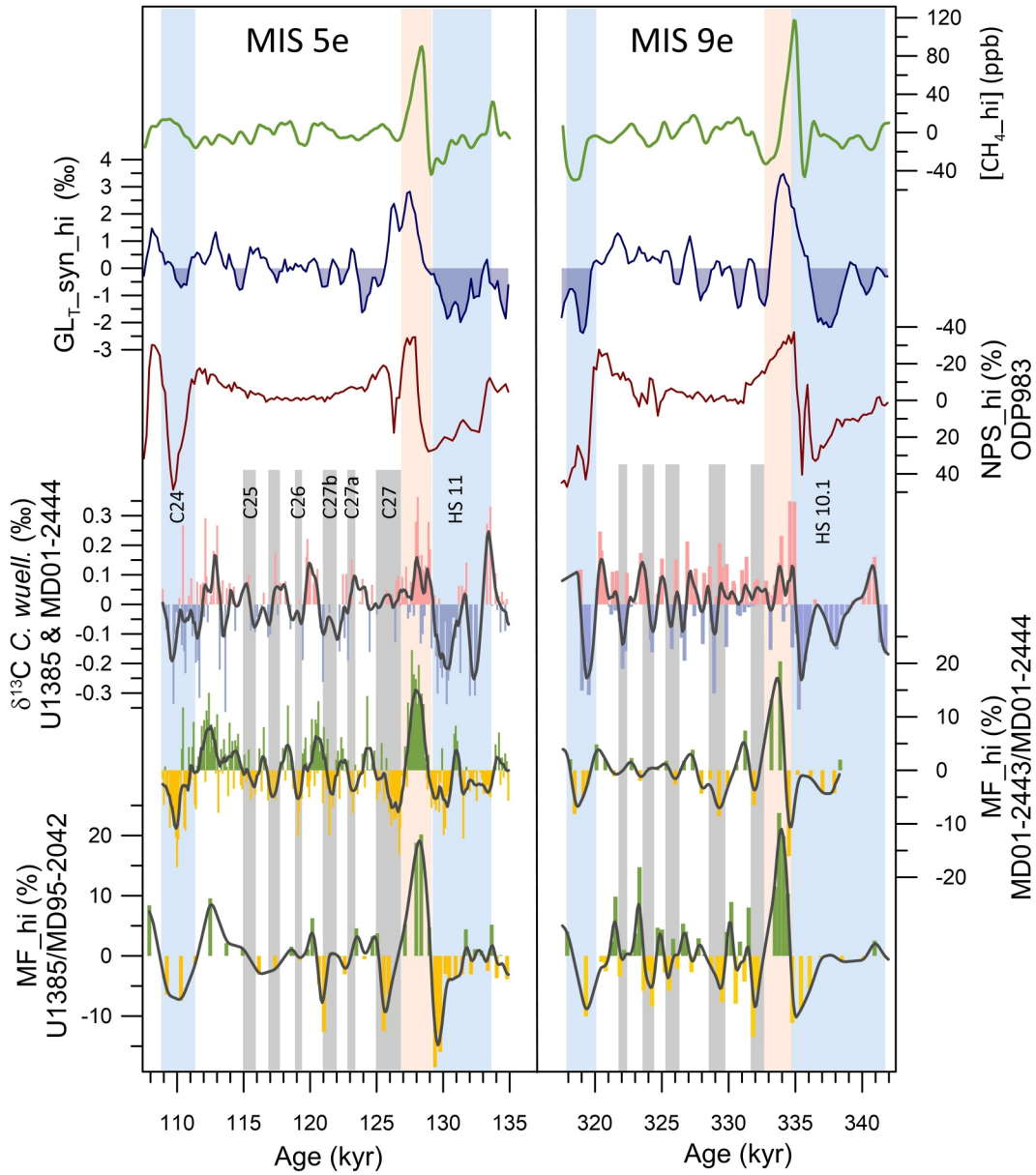

Figure 6. Suborbital climatic variability during MIS 9e and MIS 5e in the southwestern Iberian margin records. From the bottom to the top: High-frequency component of the forest pollen percentages (MF_hi) and of the benthic $\delta^{13}C$ data shown in Figure 4 estimated for all Iberian margin sites using the same procedure (colored bars: residuals of the 7 ky-Gaussian smoothing, thick line: residuals smoothed with a 0.7 ky-Gaussian filter, interpolation step of 0.3 ky for the pollen records from Site U1385, MD-95-2042 and MD01-2443, of 0.07 ky for pollen and isotopic data from core MD 01–2444 and of 0.1 ky for the isotopic record from Site U1385); High-frequency component of *Neogloboquadrina pachyderma* sinistral (or left coiling) percentages from ODP Site 983 (NPS_hi) and of the Greenland synthetic temperature signal (GLT_syn_hi) from Barker et al. (2019).

4.2.2. Variable Interglacial Intensity at Orbital-Scale

Pollen records from the SW Iberian margin clearly show that the forest reaches its greatest expansion at the beginning of MIS 5e and 9e, but as evidenced by the MF_orb component, the forest extent was clearly more limited during the MIS 9e interglacial than during MIS 5e (Figure 4). This difference in forest and winter precipitation between the two stages may not be attributed solely to the difference in insolation levels, which appears rather low. Modulation by internal forcing factors, which are known to play a fundamental role in controlling interglacial climate, must be examined (Figure 4). Since both MIS 9e and 5e are interglacial periods with

particularly reduced ice caps, we will focus on the combination of insolation and CO_2 forcing to shape the orbital-scale vegetation and precipitation response in southern Europe during intervals of enhanced global warming. We use simulations with the LOVECLIM model to estimate anomalies in vegetation cover, precipitation and temperature between MIS 5e and MIS 9e. They show higher tree fraction during MIS 5e compared to MIS 9e during the ice volume minima associated with significantly warmer annual and JJA temperatures and increased DJF precipitation (Figure 5 and Figure S6 in Supporting Information S1). These results are consistent with the vegetation and rainfall information provided by the pollen records from the SW Iberian margin. The factor separation analysis conducted in Yin and Berger (2012) shows that insolation is the dominant control of winter precipitation in Iberia at the interglacial peaks of MIS 9e and 5e, with the contribution of GHGs estimated to be much smaller. These simulation results show that the astronomical forcing, by imposing a different latitudinal and seasonal distribution of insolation, is the main forcing behind the intensification of the hydrological cycle in southern Iberia during warm periods characterized by limited residual ice caps and relatively high GHG level, such as the MIS 9e and MIS 5e. These results therefore appear to be consistent with previous works (e.g., Tzedakis, Pälike, et al., 2009; Wagner et al., 2019), which propose that variations in the winter LIG and thus the latitudinal thermal gradient play a major role in governing the atmospheric circulation of the Northern Hemisphere. They operate in particular on the position of the ITCZ and cyclone activity and trajectory, and consequently on the seasonal distribution of precipitation and its intensity in southern Europe. However, our results entail a secondary although non-negligible role of atmospheric CO_2.

4.3. A Brief Optimum in Forest Expansion at the Beginning of Both Interglacials: The Expression of the Millennial-Scale Variability

While insolation and CO_2 forcings seem to provide a satisfactory explanation for the difference in the magnitude of forest and precipitation increase between the two stages, they do not account for the brevity of the optimum as evidenced by pollen records off Iberia. The brief forest peak of MIS 9e is not a unique feature, most of the post-MBE interglacials in SW Iberia exhibit it, including MIS 5e. When the orbital component of the pollen signal is removed, the early interglacial peaks of the MF and its demise are revealed as millennial-scale variations (Figure 6). However, the driving factors behind this short-lived optimum in forest and winter precipitation remain elusive. We formulate two hypotheses for explaining the duration and magnitude of the optimum forest expansion, both of which involve millennial-scale variability and are not mutually exclusive.

4.3.1. Hypothesis 1: Optimum Duration Determined by the Demise of the Mediterranean Forest Due To Intra-Interglacial Variability

Hypothesis 1 refers to previous proposals that the short duration of the forest optimum during interglacials can be seen as the consequence of the intra-interglacial climatic variability (Tzedakis et al., 2004). According to this hypothesis, the forest that had expanded in response to orbital-scale forcing during the early millennia of the interglacials is severely reduced by an abrupt event of cooling and increased aridity. The forest does not fully recover once the event was over, possibly because of a non-return to previous climatic conditions due to the slowly changing orbital configuration.

The U1385 pollen record clearly indicates successive episodes of reduction in MF and sclerophylls during the forest interval of MIS 9e, detected at 332, 329, 326, 324, and 322 (Figures 3 and 6), suggesting that millennial cooling and drying events occurred throughout the interglacial. The forest peak ends with the occurrence of a cooling and drying event which appears to be part of the intra-interglacial climate variability that punctuated MIS 9e. Even though the MIS9e intra-interglacial variability was not evident in the pollen record of core MD01-2443, probably because of its lower time resolution, Tzedakis et al. (2004) proposed that the end of the forest optimum was caused by a millennial-scale climate change. Our new pollen record now provides evidence for millennial variability of the land climate during MIS 9e and thus may support the hypothesis proposed two decades ago. Although intra-interglacial climate variability is difficult to document during interglacial periods older than the Holocene, there is growing evidence of such variability in the literature. Millennial-scale variability of vegetation and climate in southern Europe has also been clearly identified throughout MIS 5e using the pollen record from core MD01-2444 and the Corchia speleothem record (Tzedakis et al., 2018). This study revealed a succession of increased aridity and cooling events responsible for the abrupt reductions of forests in SW Iberia. As for MIS 9e, the forest optimum ends at 127 ka with one of the millennial climatic events of MIS 5e.

Both Uk'SST record from the SW Iberian margin Site U1385 and the neighboring core MD01-2444 clearly show progressive changes in surface temperature with no clear intra-interglacial suborbital oscillations during MIS 9e (Figure 4). Such a discrepancy between pollen and SST records on this timescale has also been observed for other intervals in the SW Iberian margin, such as the MIS 5e or the MIS 11c (Oliveira et al., 2016; Tzedakis et al., 2018). Specifically, the Uk'37 and Mg/Ca SST records from core MD01-2444 do not systematically detect SST variations during the episodic reduction of MF during the last interglacial (Tzedakis et al., 2018), while planktonic assemblages from IODP Site U1385 appear to record millennial-scale decreases in annual SST of 2–3°C within MIS 5e (Singh et al., 2023). Sensitivity to moderate temperature changes (Skinner & Elderfield, 2005) and seasonal biases (Leduc et al., 2017; Williams et al., 2010) are known limitations of SST reconstructions from Uk'_{37} and planktonic foraminifera Mg/Ca. For instance, Iberian margin Uk' SSTs are intended to be reconstructions of winter temperatures because of the more stratified waters of the fall, winter and spring are the most favorable seasons for alkenone-producing coccolithophorids (Abrantes et al., 2017). These limitations are also organism dependent, as the growing seasons and depth habitats of planktonic organisms used for SST reconstructions vary and may also shift in time (e.g., Lohmann et al., 2013). In the case of intra-interglacial events, when the temperature changes are particularly moderate, vegetation in southern Iberia may be more affected by the intra-interglacial variability than planktonic organisms due to its high sensitivity to the hydroclimatic component, that is, the seasonal distribution and amount of rainfall. Modern observations also show that atmospheric modes of variability such as the NAO have a strong influence on the Iberian hydroclimate with no stationary correlation with SST over the last century (Trigo et al., 2004; Walter & Graf, 2002). In addition, oceanographic processes of the Iberian Margin may play a major role on planktonic organisms and SST variations, greater than atmospheric processes, related to the effects of summer upwelling (Haynes et al., 1993) or to the persistent influence of the Azores Current during interglacial cooling events (Girone et al., 2023). After modern observations, the correlation between SST and air temperature decreases during the winter season, especially over the eastern North Atlantic due to higher meridional temperature gradients and stronger advective processes (Cayan, 1980).

While the MIS 5e millennial-scale atmospheric events have no systematic counterpart in the Iberian margin SST record, they clearly correlate with the cooling events in the northern North Atlantic (Tzedakis et al., 2018) (Figure 6). These episodic decreases of subpolar temperature, labeled from C28 to C26, are closely associated with modest ice rafting in the North Atlantic and changes in the deep ocean circulation (Mokeddem et al., 2014; Oppo et al., 2006). The event marking the end of the MIS 5e forest peak corresponds to the North Atlantic event C27. This event is one of the strongest cooling episodes recorded in the northern North Atlantic during the last interglacial (Irvalı et al., 2012; Mokeddem et al., 2014), which resulted from a reduction in North Atlantic Deep Water (NADW) production possibly triggered by a Laurentide ice-sheet outburst flood event (Galaasen et al., 2014; Nicholl et al., 2012). Such a weakening of the AMOC had far-reaching effects on the atmospheric circulation that shaped the climate in Europe (Levy et al., 2023; Salonen et al., 2018; Tzedakis et al., 2018). As for MIS 5e, the cool and dry events of MIS 9e may be related to variability in the coupled ocean-atmosphere system of the North Atlantic. So far, it remains delicate to relate the events of forest reduction in southern Iberia to a weakening of the AMOC. However, the high-frequency component of the benthic $\delta^{13}C$ timeseries from Site U1385 clearly show variations during MIS 9e that exceed the analytical precision (±0.06‰) (Hodell et al., 2023a, 2023b) (Figures 3 and 6). It suggests an episodically reduced influence of the NADW, albeit of lesser magnitude than during major millennial-scale climatic events such as the HS10.1 event or during MIS 9d. All the drying and cooling events on land coincide with the reductions in deep-water ventilation recorded from Site U1385, excluding the event following the forest peak, at 332 ka. However, this was also the case for the last interglacial, the C27 event is not marked by a benthic $\delta^{13}C$ at the Iberian margin (Figure 6), despite the marked changes in ocean circulation in the northern North Atlantic records as mentioned above. In contrast to MIS 5e, intra-interglacial variability during MIS 9e has not yet been clearly identified in the eastern subpolar North Atlantic (Mokeddem & McManus, 2017). However, evidence for abrupt reductions in NADW ventilation in the deep North Atlantic is provided by a benthic foraminiferal record of $\delta^{13}C$ off the southern tip of Greenland (Galaasen et al., 2020). Such AMOC slowdowns have been related, although not exclusively, to episodes of increased freshwater supply favored by the sustained Greenland Ice Sheet (GIS) melting coupled with the particularly high SST off southern Greenland that occurred throughout the MIS 9e interglacial (Galaasen et al., 2020; Hatfield et al., 2016; Irvalı et al., 2020).

Episodes of AMOC weakening therefore also appear to be a plausible mechanism driving the millennial-scale event in southern Europe during MIS 9e. The impact of the reorganization of the North Atlantic circulation on the subtropical circulation during an intra-interglacial event has been demonstrated by a freshwater forcing experiment that simulates the C27 event. These simulations show a strengthening of the subtropical high-pressure system, which leads to dry conditions over southern Europe (Tzedakis et al., 2018). While further high time-resolution records in the North Atlantic and climate simulations are still needed, millennial-scale variability in the ocean-ice-atmosphere coupled system appears to be a possible cause of the demise of the early interglacial forest-climate optimum in southern Europe during warm periods of sustained ice-sheet melting.

4.3.2. Hypothesis 2: Magnitude and Duration of Optimal Forest Expansion as a Response to Non-Equilibrium Conditions Resulting From Deglacial Millennial Events

Hypothesis 2 proposes that the forest optimum can be seen as a response to a stronger-than-normal increase in winter precipitation as a consequence of a non-equilibrium state generated during the first millennia of interglacial periods by deglacial millennial-scale variability.

This second hypothesis also stems from the high-frequency component of MF signal (%MF_hi), but it is based on its highly positive values during the first millennia of interglacial periods (Figures 3 and 6, peach band). These strong values suggest that the interglacial forest peaks have a millennial character and are therefore not solely a response to orbital climate change. To test whether this result depends on the smoothing method used, we applied four different methods to remove the orbital component from the pollen percentage data (Gaussian, Moving average, Lowess and low-pass filter). We also tested whether the choice of the interpolation step and smoothing window affected the results (cf., Figure S1–S3 in Supporting Information S1). Regardless of the smoothing procedure used, the residuals obtained reveal a prominent forest peak in the high-frequency signal. This particularly warm and humid event in Iberia coincides strikingly with an anomalous warming at high latitudes in the early millennia of MIS 9e (Figure 6). This suborbital warming is described by the high-frequency component of the Greenland synthetic temperature reconstruction (GLT_syn_hi) (Barker et al., 2019). This implies that, while the temperature may not have reached its maximum at northern high latitudes, the warming was stronger than expected from the orbital-scale trend. Similar patterns are observed for MIS 5e (Figure 6).

Using the MIS 5e North Atlantic record as an example, the high-frequency component of the *N. pachyderma* s. percentages (%NPS_hi) from the ODP Site 983 shows the lowest values at the onset of the last interglacial (Barker et al., 2019), while the SST optimum in the subpolar North Atlantic is not reached until 125–124 ka (Deaney et al., 2017; Govin et al., 2012). This delayed thermal optimum in the subpolar North Atlantic has been attributed to the effect of the significant GIS ablation on the Atlantic circulation throughout Termination II to mid-MIS 5e (Carlson et al., 2008; Colville et al., 2011; Govin et al., 2012; Zhuravleva et al., 2017). However, despite continued GIS melt, the warming peak south of Greenland is attained in the early MIS 5e with warmer-than-present temperatures (Irvalı et al., 2012). In the polar North Atlantic, increased temperatures from 128.5 to 126.5 ka suggest advection of southern warm waters into the polar region in between two meltwater pulses likely associated with events C28 and C27 (Zhuravleva et al., 2017). Warming also appears to be particularly important during the early LIG in the mid-latitudes of the North Atlantic where a sharp increase in SST is recorded at the end of HS 11 (Deaney et al., 2017). On land, in western Europe, excess summer heat favored the prominent development of the oak-mixed forest during the first millennia of MIS 5e probably linked to the maintenance of strong convection in the Nordic seas despite the pronounced melting of the GIS allowing moisture and warmth to be brought to Europe (Sanchez Goñi et al., 2012).

MIS 9e records are sparser, and the history of temperature changes in the North Atlantic during this interglacial is not as well documented. The reduction of polar and Arctic foraminifera in surface waters south of Iceland occurs rapidly after the end of HS10.1 (Barker et al., 2019; Mokeddem & McManus, 2017). This suggests that the maximal advection of warm water into the eastern subpolar North Atlantic began early in the interglacial despite unabated melting of the southern GIS during most of the interglacial (Hatfield et al., 2016). At Eirik Drift, south of Greenland, as in MIS 5e, temperatures rose rapidly at the end of the deglacial millennial event, and reached the highest values since the beginning of MIS 9e (Irvalı et al., 2020). Despite the different long-term temperature history in the northern North Atlantic between MIS 5e and MIS 9e, the %NPS_hi of OPD Site 983 also displays low values during the early MIS 9e (Barker et al., 2019). This anomalous high-latitude warming coincides with the %MF_hi peak, suggesting that the climate conditions of the early MIS 9e have also an intrinsic millennial

character in the North Atlantic region and Europe. The link between the high latitude warming and a warmer, wetter southern European winter may be related to the fundamental dependency of southern European climate on the North Atlantic thermal gradient described above, favored by active convection center in the Nordic Seas. Higher-than-normal temperature increases at high latitudes would lead to a weakening of the winter latitudinal thermal gradient, originally driven by the insolation forcing, and consequently to an increase in the winter moisture supply to southern Europe.

Furthermore, as previously noticed by some authors (Sánchez Goñi et al., 2008; Tzedakis, Pälike, et al., 2009), variations in MF and atmospheric CH_4 concentrations during past climatic cycles suggested a close relationship between tropical atmospheric circulation and hydrological changes in the subtropics. Most noteworthy is that the peaks in %MF_hi, which includes an important part of the Mediterranean summer-dry taxa, coincide with the CH_4 overshoots recorded at the beginning of MIS 9e and 5e (Figure 6). Both TIV and TII are characterized by an abrupt rise in CH_4 of more than 200 ppbv in less than 400 years at 335 ka and 300 years at 129 ka (Nehrbass-Ahles et al., 2020; Schmidely et al., 2021). These increases, which occur in association with carbon dioxide jumps, have been linked to the northern shift of the ITCZ and tropical rainbelt in response to the AMOC reinvigoration at the end of HS10.1 and HS11. They are considered to be the fingerprint of a D-O-like warming: the abrupt resumption of AMOC, by forcing changes in heat distribution, would reinforce monsoonal precipitation in the northern hemisphere tropics, and thus trigger sudden increased methane emissions from wetlands (Nehrbass-Ahles et al., 2020; Schmidely et al., 2021). Modeling experiments have shown that the abrupt deep-water reorganization in the North Atlantic that occurred at the end of millennial-scale deglacial events is critical for generating the observed rapid northward displacement of the ITCZ and increased monsoonal rainfall in Africa (Menviel et al., 2021). As the intensification of the tropical summer circulation is accompanied by a strengthening of the descending branch of the Hadley cell and thus of the subtropical highs, the enhancement of summer dryness in Iberia in early MIS 9e and 5e in response to the abrupt AMOC reinvigoration appears to be a reasonable mechanism.

Therefore, records from the tropics to the northern North Atlantic and Europe point to evidence that the climate change at the end of the terminal millennial events and the climate that prevailed during the first millennia of both MIS 9e and 5e are shaped by the millennial-scale variability. According to Barker et al. (2019), the anomalous early interglacial warming at the high latitudes reflects a state of non-equilibrium generated by the change in ocean circulation that followed the abrupt millennial-scale events of the Terminations and persisted for a few millennia. The excess heat in the North Atlantic is thought to have been delivered to the high latitudes by an abnormally strong AMOC at the beginning of the interglacial periods. These conditions would result from a transient state during which the Nordic heat pump has been reactivated although not at their maximal intensity while the boreal heat pump, the prevailing mode of the glacial stages, is still strong (Barker et al., 2019). The recent εNd record of MIS 5e from ODP Site 1063 located in the eastern subtropical North Atlantic supports this view. It indicates that the AMOC abruptly resumed at the end of HS11 with an overshoot during the early Last Interglacial that lasted several millennia (Deaney et al., 2017). This unexpected AMOC overshoot may result from a deepening and strengthening of deep-water formed in southern regions of convection, probably in the NW Atlantic (Deaney et al., 2017). Deep-water formation in the NE Atlantic was also reactivated although remained quite restricted and shallow until 124 ka, probably as a consequence of the strong GIS melting in the early MIS 5e (Deaney et al., 2017; Galaasen et al., 2014; Govin et al., 2012). Results from LOVECLIM simulations also showed that enhanced GIS melting during the early Last Interglacial period may have inhibited the convection centers of northern Iceland and Labrador Sea in the early MIS 5e but did not disturbed that of the Nordic Seas (Sanchez Goñi et al., 2012). So far, there is no record of an AMOC overshoot in the early MIS 9e. Records of the oceanic circulation in the subpolar latitudes show that NADW formation also resumed during the TIV after the HS 10.1 event. However, in contrast to MIS 5e, only depths deeper than 2,000 m appear to have been ventilated while intermediate depths remained poorly ventilated and that this circulation pattern in the subpolar North Atlantic remained prevailing until the end of MIS 9e (Mokeddem & McManus, 2017). The benthic $\delta^{13}C$_hi from Site U1385, like that of MD01-2444 for MS 5e, shows an abrupt, above-normal strengthening of the North Atlantic deep-water circulation during the first millennia of the interglacial (Figure 6). The abrupt circulation shift at the end of the terminal millennial event, accompanied by pronounced GIS melting, may have generated similar instability or transient oceanic circulation mode at the beginning of both MIS 5e and MIS 9e interglacial periods.

We then propose that the non-equilibrium state in the AMOC generated at the end of the terminal deglacial Heinrich events exacerbated the winter moisture supply to southern Europe and the summer warming and drying dictated by the insolation forcing during early MIS 5e and 9e. Such a pattern may not be limited to these

interglacial stages, as anomalously strong warming at high latitudes has been detected at the onset of all interglacials of the last 800 ky (Barker et al., 2019). For instance, the particularly high forest expansion of the Holocene (Chabaud et al., 2014) also appears to be synchronous with high values of GLT_syn_hi and may contribute to the prominent forest expansion. The vegetation record of the Iberian Margin emphasizes that interglacial intensity and drivers cannot be fully understood only through the lens of orbital-scale climate variability, millennial-scale variability likely played a prominent role in shaping the interglacial climate optima.

5. Conclusions

The aim of this work was to characterize the vegetation and climate changes in southern Europe during warm interglacial periods that occurred after the Mid-Brunhes event. We have presented new pollen and SST records from the Iberian Margin IODP Site U1385 for the interval 317–342 ka, encompassing the MIS 9e interglacial. This new pollen record shows that the MF expanded over an interval of more than 12 ky, bracketed by the millennial-scale cooling events of TIV and MIS 9d associated with iceberg discharges in the North Atlantic. In agreement with previous records, the forests of southern Iberia reached their maximum expansion during the first millennia of the MIS 9e interglacial. This suggests a stronger seasonality of precipitation with increased winter moisture availability when the Northern Hemisphere summers are close to perihelion, as previously observed for the last interglacial. Comparison of MIS 9e with MIS 5e, another interglacial period of particularly strong high-latitude warming and reduced ice caps, using data and model simulations, shows that subtle differences in the seasonal and latitudinal insolation distribution produced marked difference in the orbital-scale response of the hydrological cycle and vegetation in southwestern Europe. The higher CO_2 forcing during MIS 9e attenuates this difference but does not offset the climate response to the insolation forcing. Furthermore, the continental and marine records from Site U1385 provide new evidence that intra-interglacial climate variability is a persistent feature of past interglacials in southern Europe, probably linked to millennial-scale oscillations in deep-sea circulation. The high-frequency component of the MF time series highlights the early interglacial forest maxima as a prominent suborbital event and therefore that the duration and intensity of the interglacial maxima cannot be explained solely by forcing factors acting at the orbital scale. As suggested previously, the early demise of the forest with no return to previous conditions related to moving boundary conditions may have been promoted by cooling and drying events in response to AMOC weakening. Specifically, we proposed that the brief and pronounced forest and precipitation maxima recorded in southern Iberia during the early part of the interglacials may be viewed as a response to the non-equilibrium conditions over the first millennia of the interglacial periods generated by the millennial-scale deglacial events. The early interglacial anomalous high-latitude conditions, as recorded in the Greenland synthetic temperature record, would have exacerbated the weakening of the winter latitudinal thermal gradient driven by orbital-scale forcing, and hence the moisture supply to southern Europe. Thus, during warm periods of sustained ice-sheet melting, the interplay between orbital and millennial-scale variability therefore appears to be central to explaining interglacial intensity. Further research is needed to verify whether the co-occurrence of anomalous high-latitude warming and forest overshoot in southern Iberia during the first millennia of interglacial periods is a pervasive relationship throughout the Mid-to Late Pleistocene.

Data Availability Statement

All new data from IODP Site U1385 presented in this manuscript are available online in the PANGAEA data repository. Three data sets are provided: raw pollen data (Desprat et al., 2024b), pollen percentages (Desprat et al., 2024c) and biomarker data (Uk'_{37} SST and %C37) (Desprat et al., 2024a).

Acknowledgments
This work used samples provided by the International Ocean Discovery Program. We express gratitude to the IODP Expedition 339 drilling crew, ship crew, technical and scientific staff of the Joides Resolution, to the expedition PIs and to the curator of the Bremen Core Center and his team. We thank Ludovic Devaux and Muriel Georget for the curation of the samples at EPOC and their assistance in the lab. We are also grateful to Vincent Hanquiez (EPOC) for designing and realizing the maps presented in this work. Financial support was provided by the French research program LEFE (INSU-CNRS, projects *WarmClim* and *PuLSE*), IODP France and the EPHE (Gauthier Guillem's MSc. grant) to SD, MFSG and GG to realize the palynological work at EPOC. The ocean surface hydrological analysis carried out by TR at IPMA and JG at IDAEA. It was funded by the Portuguese Foundation for Science and Technology—FCT, through the *WarmWorld* project (PTDC/CTA-GEO/29897/2017), CCMAR FCT Research Unit—project UIDB/04326/2020, and IPMA's Biogeochemistry Lab equipment was supported by EMSO-PT—PINFRA/22157/2016. Computational resources of the model simulations were provided by the supercomputing facilities of the Université catholique de Louvain (CISM/UCL) and the Consortium des Équipements de Calcul Intensif en Fédération Wallonie Bruxelles (CÉCI) funded by F.R.S.-FNRS under convention 2.5020.11.

References

Abrantes, F., Rodrigues, T., Rufino, M., Salgueiro, E., Oliveira, D., Gomes, S., et al. (2017). The climate of the Common Era off the Iberian Peninsula. *Climate of the Past*, *13*(12), 1901–1918. https://doi.org/10.5194/cp-13-1901-2017

Anderson, L., Wahl, D. B., & Bhattacharya, T. (2022). Understanding rates of change: A case study using fossil pollen records from California to assess the potential for and challenges to a regional data synthesis. *Quaternary International*, *621*, 26–36. https://doi.org/10.1016/j.quaint.2020.04.044

Barker, S., & Knorr, G. (2021). Millennial scale feedbacks determine the shape and rapidity of glacial termination. *Nature Communications*, *12*(1), 2273. https://doi.org/10.1038/s41467-021-22388-6

Barker, S., Knorr, G., Conn, S., Lordsmith, S., Newman, D., & Thornalley, D. (2019). Early interglacial legacy of deglacial climate instability. *Paleoceanography and Paleoclimatology*, *34*(8), 1455–1475. https://doi.org/10.1029/2019PA003661

Barker, S., Knorr, G., Edwards, R. L., Parrenin, F., Putnam, A. E., Skinner, L. C., et al. (2011). 800,000 years of abrupt climate variability. *Science*, *334*(6054), 347–351. https://doi.org/10.1126/science.1203580

Bazin, L., Landais, A., Lemieux-Dudon, B., Toyé Mahamadou Kele, H., Veres, D., Parrenin, F., et al. (2013). An optimized multi-proxy, multi-site Antarctic ice and gas orbital chronology (AICC2012): 120–800 ka. *Climate of the Past*, *9*(4), 1715–1731. https://doi.org/10.5194/cp-9-1715-2013

Bereiter, B., Eggleston, S., Schmitt, J., Nehrbass-Ahles, C., Stocker, T. F., Fischer, H., et al. (2015). Revision of the EPICA Dome C CO_2 record from 800 to 600 kyr before present. *Geophysical Research Letters*, *42*(2), 542–549. https://doi.org/10.1002/2014gl061957

Berger, A., & Loutre, M. F. (1991). Insolation values for the climate of the last 10 million years. *Quaternary Science Reviews*, *10*(4), 297–317. https://doi.org/10.1016/0277-3791(91)90033-q

Blanco Castro, E., Casado González, M. A., Costa Tenorio, M., Escribano Bombín, R., García Antón, M., Génova Fuster, M., et al. (1997). *Los bosques ibéricos*. Planeta.

Broecker, W. S., & van Donk, J. (1970). Insolation changes, ice volumes, and the O^{18} record in deep-sea cores. *Reviews of Geophysics*, *8*(1), 169–198. https://doi.org/10.1029/RG008i001p00169

Carlson, A. E., Stoner, J. S., Donnelly, J. P., & Hillaire-Marcel, C. (2008). Response of the southern Greenland Ice Sheet during the last two deglaciations. *Geology*, *36*(5), 359. https://doi.org/10.1130/G24519A.1

Cayan, D. R. (1980). Large-scale relationships between sea surface temperature and surface air temperature. *Monthly Weather Review*, *108*(9), 1293–1301. https://doi.org/10.1175/1520-0493(1980)108<1293:LSRBSS>2.0.CO;2

Chabaud, L., Sánchez Goñi, M. F., Desprat, S., & Rossignol, L. (2014). Land-sea climatic variability in the eastern North Atlantic subtropical region over the last 14,200 years: Atmospheric and oceanic processes at different timescales. *The Holocene*, *24*(7), 787–797. https://doi.org/10.1177/0959683614530439

Colville, E. J., Carlson, A. E., Beard, B. L., Hatfield, R. G., Stoner, J. S., Reyes, A. V., & Ullman, D. J. (2011). Sr-Nd-Pb isotope evidence for ice-sheet presence on southern Greenland during the Last Interglacial. *Science*, *333*(6042), 620–623. https://doi.org/10.1126/science.1204673

Davis, B. A. S., & Brewer, S. (2009). Orbital forcing and role of the latitudinal insolation/temperature gradient. *Climate Dynamics*, *32*(2–3), 143–165. https://doi.org/10.1007/s00382-008-0480-9

Deaney, E. L., Barker, S., & van de Flierdt, T. (2017). Timing and nature of AMOC recovery across Termination 2 and magnitude of deglacial CO_2 change. *Nature Communications*, *8*(1), 14595. https://doi.org/10.1038/ncomms14595

Desprat, S., Oliveira, D., Naughton, F., & Goñi, M. F. S. (2017). Pollen in marine sedimentary archives, a key for climate studies: The example of past warm periods. *Quaternaire*, *28*(2), 259–269. https://doi.org/10.4000/quaternaire.8102

Desprat, S., Rodrigues, T., Guillem, G., Sánchez Goñi, M. F., Yin, Q., & Grimalt, J. O. (2024a). Biomarker data (Uk'_{37} SST and %C37:4) from IODP Site 339-U1385 [Dataset]. *PANGAEA*. https://doi.org/10.1594/PANGAEA.967273

Desprat, S., Rodrigues, T., Guillem, G., Sánchez Goñi, M. F., Yin, Q., & Grimalt, J. O. (2024b). Pollen counts from IODP Site 339-U1385 [Dataset]. *PANGAEA*. https://doi.org/10.1594/PANGAEA.967271

Desprat, S., Rodrigues, T., Guillem, G., Sánchez Goñi, M. F., Yin, Q., & Grimalt, J. O. (2024c). Pollen percentages from IODP Site 339-U1385 [Dataset]. *PANGAEA*. https://doi.org/10.1594/PANGAEA.967272

Desprat, S., Sanchez Goñi, M. F., McManus, J. F., Duprat, J., & Cortijo, E. (2009). Millennial-scale climatic variability between 340 000 and 270 000 years ago in SW Europe: Evidence from a NW Iberian margin pollen sequence. *Climate of the Past*, *5*(1), 53–72. https://doi.org/10.5194/cp-5-53-2009

Desprat, S., Sánchez Goñi, M. F., Naughton, F., Turon, J. L., Duprat, J., Malaizé, B., et al. (2007). Climate variability of the last five isotopic interglacials: Direct land-sea-ice correlation from the multiproxy analysis of North-Western Iberian margin deep-sea cores. In M. C. M. F. S. G. Frank Sirocko & L. Thomas (Eds.), *Developments in Quaternary Sciences* (Vol. 7, pp. 375–386). Elsevier. https://doi.org/10.1016/S1571-0866(07)80050-9

Dorai-Raj, S. (2022). binom: binomial confidence intervals for several parameterizations (Version R package version 1.1-1.1). Retrieved from https://CRAN.R-project.org/package=binom

Galaasen, E. V., Ninnemann, U. S., Irvalı, N., Kleiven, H. K. F., Rosenthal, Y., Kissel, C., & Hodell, D. A. (2014). Rapid reductions in North Atlantic Deep Water during the peak of the last interglacial period. *Science*, *343*(6175), 1129–1132. https://doi.org/10.1126/science.1248667

Galaasen, E. V., Ninnemann, U. S., Kessler, A., Irvalı, N., Rosenthal, Y., Tjiputra, J., et al. (2020). Interglacial instability of North Atlantic Deep Water ventilation. *Science*, *367*(6485), 1485–1489. https://doi.org/10.1126/science.aay6381

Girone, A., De Astis, A., Sierro, F. J., Hernández-Almeida, I., Garcia, M. A., Sánchez Goñi, M. F., et al. (2023). Planktonic foraminifera response to orbital and millennial-scale climate variability at the southern Iberian Margin (IODP Site U1385) during Marine Isotope Stages 20 and 19. *Palaeogeography, Palaeoclimatology, Palaeoecology*, *615*, 111450. https://doi.org/10.1016/j.palaeo.2023.111450

Govin, A., Braconnot, P., Capron, E., Cortijo, E., Duplessy, J.-C., Jansen, E., et al. (2012). Persistent influence of ice sheet melting on high northern latitude climate during the early Last Interglacial. *Climate of the Past*, *8*(2), 483–507. https://doi.org/10.5194/cp-8-483-2012

Grant, K. M., Rohling, E. J., Bar-Matthews, M., Ayalon, A., Medina-Elizalde, M., Ramsey, C. B., et al. (2012). Rapid coupling between ice volume and polar temperature over the past 150,000 years. *Nature*, *491*(7426), 744–747. https://doi.org/10.1038/nature11593

Hamilton, N. (2015). smoother: Functions Relating to the Smoothing of Numerical Data (Version R package version 1.1). Retrieved from https://CRAN.R-project.org/package=smoother

Hatfield, R. G., Reyes, A. V., Stoner, J. S., Carlson, A. E., Beard, B. L., Winsor, K., & Welke, B. (2016). Interglacial responses of the southern Greenland ice sheet over the last 430,000 years determined using particle-size specific magnetic and isotopic tracers. *Earth and Planetary Science Letters*, *454*, 225–236. https://doi.org/10.1016/j.epsl.2016.09.014

Haynes, R., Barton, E. D., & Pilling, I. (1993). Development, persistence, and variability of upwelling filaments off the Atlantic coast of the Iberian Peninsula. *Journal of Geophysical Research*, *98*(C12), 22681–22692. https://doi.org/10.1029/93JC02016

Heusser, L. E., & Balsam, W. L. (1977). Pollen distribution in the N.E. Pacific Ocean. *Quaternary Research*, *7*(1), 45–62. https://doi.org/10.1016/0033-5894(77)90013-8

Hodell, D. A., Crowhurst, S., Skinner, L., Tzedakis, P. C., Margari, V., Channell, J. E. T., et al. (2013). Response of Iberian Margin sediments to orbital and suborbital forcing over the past 420 ka: Iberian margin paleoceanography. *Paleoceanography*, *28*(1), 185–199. https://doi.org/10.1002/palo.20017

Hodell, D. A., Crowhurst, S. J., Lourens, L., Margari, V., Nicolson, J., Rolfe, J. E., et al. (2023a). A 1.5-million-year record of orbital and millennial climate variability in the North Atlantic. *Climate of the Past*, *19*(3), 607–636. https://doi.org/10.5194/cp-19-607-2023

Hodell, D. A., Crowhurst, S. J., Lourens, L. J., Margari, V., Nicolson, J., Rolfe, J. E., et al. (2023b). Benthic and planktonic oxygen and carbon isotopes and XRF data at IODP Site U1385 and core MD01-2444 from 0 to 1.5 Ma [Dataset]. *PANGAEA*. https://doi.org/10.1594/PANGAEA.951401

Hodell, D. A., Lourens, L., Crowhurst, S., Konijnendijk, T., Tjallingii, R., Jiménez-Espejo, F., et al. (2015). A reference time scale for Site U1385 (Shackleton Site) on the SW Iberian Margin. *Global and Planetary Change*, *133*, 49–64. https://doi.org/10.1016/j.gloplacha.2015.07.002

Hodell, D. A., Lourens, L., Stow, D. A. V., Hernández-Molina, J., Alvarez Zarikian, C. A., & the Shackleton Site Project Members. (2013). The "Shackleton Site" (IODP Site U1385) on the Iberian Margin. *Scientific Drilling*, *16*, 13–19. https://doi.org/10.5194/sd-16-13-2013

Irvalı, N., Galaasen, E. V., Ninnemann, U. S., Rosenthal, Y., Born, A., & Kleiven, H. K. F. (2020). A low climate threshold for south Greenland Ice Sheet demise during the Late Pleistocene. *Proceedings of the National Academy of Sciences*, *117*(1), 190–195. https://doi.org/10.1073/pnas.1911902116

Irvalı, N., Ninnemann, U. S., Galaasen, E. V., Rosenthal, Y., Kroon, D., Oppo, D. W., et al. (2012). Rapid switches in subpolar North Atlantic hydrography and climate during the Last Interglacial (MIS 5e): Hydrography and climate of MIS 5e. *Paleoceanography*, *27*(2), PA2207. https://doi.org/10.1029/2011PA002244

Kousis, I., Koutsodendris, A., Peyron, O., Leicher, N., Francke, A., Wagner, B., et al. (2018). Centennial-scale vegetation dynamics and climate variability in SE Europe during Marine Isotope Stage 11 based on a pollen record from Lake Ohrid. *Quaternary Science Reviews*, *190*, 20–38. https://doi.org/10.1016/j.quascirev.2018.04.014

Koutsodendris, A., Dakos, V., Fletcher, W. J., Knipping, M., Kotthoff, U., Milner, A. M., et al. (2023). Atmospheric CO_2 forcing on Mediterranean biomes during the past 500 kyrs. *Nature Communications*, *14*(1), 1664. https://doi.org/10.1038/s41467-023-37388-x

Kutzbach, J. E., Chen, G., Cheng, H., Edwards, R. L., & Liu, Z. (2014). Potential role of winter rainfall in explaining increased moisture in the Mediterranean and Middle East during periods of maximum orbitally-forced insolation seasonality. *Climate Dynamics*, *42*(3–4), 1079–1095. https://doi.org/10.1007/s00382-013-1692-1

Lang, N., & Wolff, E. W. (2011). Interglacial and glacial variability from the last 800 ka in marine, ice and terrestrial archives. *Climate of the Past*, *7*(2), 361–380. https://doi.org/10.5194/cp-7-361-2011

Leduc, G., Garidel-Thoron, T. D., Kaiser, J., Bolton, C., & Contoux, C. (2017). Databases for sea surface paleotemperature based on geochemical proxies from marine sediments: Implications for model-data comparisons. *Quaternaire*, *28*(2), 201–216. https://doi.org/10.4000/quaternaire.8034

Levy, E. J., Vonhof, H. B., Bar-Matthews, M., Martínez-García, A., Ayalon, A., Matthews, A., et al. (2023). Weakened AMOC related to cooling and atmospheric circulation shifts in the last interglacial Eastern Mediterranean. *Nature Communications*, *14*(1), 5180. https://doi.org/10.1038/s41467-023-40880-z

Lohmann, G., Pfeiffer, M., Laepple, T., Leduc, G., & Kim, J.-H. (2013). A model-data comparison of the Holocene global sea surface temperature evolution. *Climate of the Past*, *9*(4), 1807–1839. https://doi.org/10.5194/cp-9-1807-2013

Loidi, J., Biurrun, I., Campos, J. A., García-Mijangos, I., & Herrera, M. (2007). A survey of heath vegetation of the Iberian Peninsula and Northern Morocco: A biogeographic and bioclimatic approach. *Phytocoenologia*, *37*(3–4), 341–370. https://doi.org/10.1127/0340-269X/2007/0037-0341

Loidi, J., Biurrun, I., Campos, J. A., García-Mijangos, I., & Herrera, M. (2010). A biogeographical analysis of the European Atlantic lowland heathlands: Biogeographical analysis of European Atlantic lowland heathlands. *Journal of Vegetation Science*, *21*(5), 832–842. https://doi.org/10.1111/j.1654-1103.2010.01204.x

Lüthi, D., Le Floch, M., Bereiter, B., Blunier, T., Barnola, J.-M., Siegenthaler, U., et al. (2008). High-resolution carbon dioxide concentration record 650,000–800,000 years before present. *Nature*, *453*(7193), 379–382. https://doi.org/10.1038/nature06949

Martrat, B., Grimalt, J. O., Shackleton, N. J., de Abreu, L., Hutterli, M. A., & Stocker, T. F. (2007). Four climate cycles of recurring deep and surface water destabilizations on the Iberian margin. *Science*, *317*(5837), 502–507. https://doi.org/10.1126/science.1139994

Masson-Delmotte, V., Stenni, B., Pol, K., Braconnot, P., Cattani, O., Falourd, S., et al. (2010). EPICA Dome C record of glacial and interglacial intensities. *Quaternary Science Reviews*, *29*(1–2), 113–128. https://doi.org/10.1016/j.quascirev.2009.09.030

McManus, J. F., Oppo, D. W., & Cullen, J. L. (1999). A 0.5-million-year record of millennial-scale climate variability in the North Atlantic. *Science*, *283*(5404), 971–975. https://doi.org/10.1126/science.283.5404.971

Menviel, L., Govin, A., Avenas, A., Meissner, K. J., Grant, K. M., & Tzedakis, P. C. (2021). Drivers of the evolution and amplitude of African Humid Periods. *Communications Earth & Environment*, *2*(1), 237. https://doi.org/10.1038/s43247-021-00309-1

Mokeddem, Z., & McManus, J. F. (2017). Insights into North Atlantic deep water formation during the peak interglacial interval of Marine Isotope Stage 9 (MIS 9). *Climate Dynamics*, *49*(9–10), 3193–3208. https://doi.org/10.1007/s00382-016-3505-9

Mokeddem, Z., McManus, J. F., & Oppo, D. W. (2014). Oceanographic dynamics and the end of the last interglacial in the subpolar North Atlantic. *Proceedings of the National Academy of Sciences*, *111*(31), 11263–11268. https://doi.org/10.1073/pnas.1322103111

Morales-Molino, C., Devaux, L., Georget, M., Hanquiez, V., & Sánchez Goñi, M. F. (2020). Modern pollen representation of the vegetation of the Tagus Basin (central Iberian Peninsula). *Review of Palaeobotany and Palynology*, *276*, 104193. https://doi.org/10.1016/j.revpalbo.2020.104193

Myllymäki, M., & Mrkvička, T. (2023). *GET: Global envelopes in R*. arXiv. Retrieved from http://arxiv.org/abs/1911.06583

Naughton, F., Sanchez Goñi, M. F., Desprat, S., Turon, J. L., Duprat, J., Malaizé, B., et al. (2007). Present-day and past (last 25 000 years) marine pollen signal off western Iberia. *Marine Micropaleontology*, *62*(2), 91–114. https://doi.org/10.1016/j.marmicro.2006.07.006

Nehrbass-Ahles, C., Shin, J., Schmitt, J., Bereiter, B., Joos, F., Schilt, A., et al. (2020). Abrupt CO_2 release to the atmosphere under glacial and early interglacial climate conditions. *Science*, *369*(6506), 1000–1005. https://doi.org/10.1126/science.aay8178

Nicholl, J. A. L., Hodell, D. A., Naafs, B. D. A., Hillaire-Marcel, C., Channell, J. E. T., & Romero, O. E. (2012). A Laurentide outburst flooding event during the last interglacial period. *Nature Geoscience*, *5*(12), 901–904. https://doi.org/10.1038/ngeo1622

Oksanen, J., Simpson, G., Blanchet, F., Kindt, R., Legendre, P., Minchin, P., et al. (2022). vegan: Community Ecology Package (Version R package version 2.6-2). Retrieved from https://CRAN.R-project.org/package=vegan

Oliveira, D., Desprat, S., Rodrigues, T., Naughton, F., Hodell, D., Trigo, R., et al. (2016). The complexity of millennial-scale variability in southwestern Europe during MIS 11. *Quaternary Research*, *86*(3), 373–387. https://doi.org/10.1016/j.yqres.2016.09.002

Oliveira, D., Desprat, S., Yin, Q., Naughton, F., Trigo, R., Rodrigues, T., et al. (2018). Unraveling the forcings controlling the vegetation and climate of the best orbital analogues for the present interglacial in SW Europe. *Climate Dynamics*, *51*(1–2), 667–686. https://doi.org/10.1007/s00382-017-3948-7

Oppo, D. W., McManus, J. F., & Cullen, J. L. (2006). Evolution and demise of the Last Interglacial warmth in the subpolar North Atlantic. *Quaternary Science Reviews*, *25*(23–24), 3268–3277. https://doi.org/10.1016/j.quascirev.2006.07.006

Overpeck, J. T., Webb, T., III, & Prentice, I. C. (1985). Quantitative interpretation of fossil pollen spectra: Dissimilarity coefficients and the method of modern analogs. *Quaternary Research*, *23*(1), 87–108. https://doi.org/10.1016/0033-5894(85)90074-2

Pailler, D., & Bard, E. (2002). High frequency palaeoceanographic changes during the past 140 000 yr recorded by the organic matter in sediments of the Iberian Margin. *Palaeogeography, Palaeoclimatology, Palaeoecology*, *181*(4), 431–452. https://doi.org/10.1016/S0031-0182(01)00444-8

Past Interglacials Working Group of Pages. (2016). Interglacials of the last 800,000 years. *Reviews of Geophysics*, *54*(1), 162–219. https://doi.org/10.1002/2015rg000482

Peinado Lorca, M., & Martínez-Parras, J. M. (1987). Castilla-La Mancha. In M. Peinado Lorca & S. Rivas-Martinez (Eds.), *La vegetación de España*, *Alcala de Henares* (pp. 163–196). Universidad de Alcalá de Henares.

Pérez, F. F., Castro, C. G., Álvarez–Salgado, X. A., & Ríos, A. F. (2001). Coupling between the Iberian basin — Scale circulation and the Portugal boundary current system: A chemical study. *Deep Sea Research Part I: Oceanographic Research Papers*, *48*(6), 1519–1533. https://doi.org/10.1016/S0967-0637(00)00101-1

Regattieri, E., Zanchetta, G., Isola, I., Bajo, P., Perchiazzi, N., Drysdale, R. N., et al. (2018). A MIS 9/MIS 8 speleothem record of hydrological variability from Macedonia (F.Y.R.O.M.). *Global and Planetary Change*, *162*, 39–52. https://doi.org/10.1016/j.gloplacha.2018.01.003

Reille, M., & de Beaulieu, J.-L. (1995). Long Pleistocene pollen records from the Praclaux Crater, South-Central France. *Quaternary Research*, *44*(2), 205–215. https://doi.org/10.1006/qres.1995.1065

Rodrigues, T., Alonso-García, M., Hodell, D. A., Rufino, M., Naughton, F., Grimalt, J. O., et al. (2017). A 1-Ma record of sea surface temperature and extreme cooling events in the North Atlantic: A perspective from the Iberian Margin. *Quaternary Science Reviews*, *172*, 118–130. https://doi.org/10.1016/j.quascirev.2017.07.004

Rohling, E. J., Hibbert, F. D., Grant, K. M., Galaasen, E. V., Irvalı, N., Kleiven, H. F., et al. (2019). Asynchronous Antarctic and Greenland ice-volume contributions to the last interglacial sea-level highstand. *Nature Communications*, *10*(1), 9. https://doi.org/10.1038/s41467-019-12874-3

Roucoux, K. H., Tzedakis, P. C., de Abreu, L., & Shackleton, N. J. (2006). Climate and vegetation changes 180,000 to 345,000 years ago recorded in a deep-sea core off Portugal. *Earth and Planetary Science Letters*, *249*(3–4), 307–325. https://doi.org/10.1016/j.epsl.2006.07.005

Sadori, L., Koutsodendris, A., Panagiotopoulos, K., Masi, A., Bertini, A., Combourieu-Nebout, N., et al. (2016). Pollen-based paleoenvironmental and paleoclimatic change at Lake Ohrid (south-eastern Europe) during the past 500 ka. *Biogeosciences*, *13*(5), 1423–1437. https://doi.org/10.5194/bg-13-1423-2016

Salgueiro, E., Voelker, A., Abrantes, F., Meggers, H., Pflaumann, U., Lončarić, N., et al. (2008). Planktonic foraminifera from modern sediments reflect upwelling patterns off Iberia: Insights from a regional transfer function. *Marine Micropaleontology*, *66*(3–4), 135–164. https://doi.org/10.1016/j.marmicro.2007.09.003

Salonen, J. S., Helmens, K. F., Brendryen, J., Kuosmanen, N., Väliranta, M., Goring, S., et al. (2018). Abrupt high-latitude climate events and decoupled seasonal trends during the Eemian. *Nature Communications*, *9*(1), 2851. https://doi.org/10.1038/s41467-018-05314-1

Sanchez Goñi, M. F., Bakker, P., Desprat, S., Carlson, A. E., Van Meerbeeck, C. J., Peyron, O., et al. (2012). European climate optimum and enhanced Greenland melt during the last interglacial. *Geology*, *40*(7), 627–630. https://doi.org/10.1130/g32908.1

Sánchez Goñi, M. F., Bard, E., Landais, A., Rossignol, L., & d'Errico, F. (2013). Air–sea temperature decoupling in western Europe during the last interglacial–glacial transition. *Nature Geoscience*, *6*(10), 837–841. https://doi.org/10.1038/ngeo1924

Sánchez Goñi, M. F., Desprat, S., Fletcher, W. J., Morales-Molino, C., Naughton, F., Oliveira, D., et al. (2018). Pollen from the deep-sea: A breakthrough in the mystery of the Ice Ages. *Frontiers in Plant Science*, *9*, 38. https://doi.org/10.3389/fpls.2018.00038

Sánchez Goñi, M. F., Eynaud, F., Turon, J.-L., & Shackleton, N. J. (1999). High resolution palynological record off the Iberian margin: Direct land-sea correlation for the Last Interglacial complex. *Earth and Planetary Science Letters*, *171*(1), 123–137. https://doi.org/10.1016/s0012-821x(99)00141-7

Sánchez Goñi, M. F., Landais, A., Fletcher, W. J., Naughton, F., Desprat, S., & Duprat, J. (2008). Contrasting impacts of Dansgaard-Oeschger events over a western European latitudinal transect modulated by orbital parameters. *Quaternary Science Reviews*, *27*(11–12), 1136–1151. https://doi.org/10.1016/j.quascirev.2008.03.003

Sánchez Goñi, M. F., Rodrigues, T., Hodell, D. A., Polanco-Martínez, J. M., Alonso-García, M., Hernández-Almeida, I., et al. (2016). Tropically-driven climate shifts in southwestern Europe during MIS 19, a low eccentricity interglacial. *Earth and Planetary Science Letters*, *448*, 81–93. https://doi.org/10.1016/j.epsl.2016.05.018

Sassoon, D., Lebreton, V., Combourieu-Nebout, N., Peyron, O., & Moncel, M.-H. (2023). Palaeoenvironmental changes in the southwestern Mediterranean (ODP site 976, Alboran sea) during the MIS 12/11 transition and the MIS 11 interglacial and implications for hominin populations. *Quaternary Science Reviews*, *304*, 108010. https://doi.org/10.1016/j.quascirev.2023.108010

Schmidely, L., Nehrbass-Ahles, C., Schmitt, J., Han, J., Silva, L., Shin, J., et al. (2021). CH_4 and N_2O fluctuations during the penultimate deglaciation. *Climate of the Past*, *17*(4), 1627–1643. https://doi.org/10.5194/cp-17-1627-2021

Shackleton, N. J., Sanchez Goñi, M. F., Pailler, D., & Lancelot, Y. (2003). Marine isotope substage 5e and the Eemian interglacial. *Global and Planetary Change*, *36*(3), 151–155. https://doi.org/10.1016/s0921-8181(02)00181-9

Singh, H., Singh, A. D., Tripathi, R., Singh, P., Verma, K., Voelker, A. H. L., & Hodell, D. A. (2023). Centennial-millennial scale ocean-climate variability in the northeastern Atlantic across the last three terminations. *Global and Planetary Change*, *223*, 104100. https://doi.org/10.1016/j.gloplacha.2023.104100

Skinner, L. C., & Elderfield, H. (2005). Constraining ecological and biological bias in planktonic foraminiferal Mg/Ca and $\delta^{18}O_{cc}$: A multispecies approach to proxy calibration testing. *Paleoceanography*, *20*(1), PA1015. https://doi.org/10.1029/2004PA001058

Sun, Y., McManus, J. F., Clemens, S. C., Zhang, X., Vogel, H., Hodell, D. A., et al. (2021). Persistent orbital influence on millennial climate variability through the Pleistocene. *Nature Geoscience*, *14*(11), 812–818. https://doi.org/10.1038/s41561-021-00794-1

Trigo, R. M., Pozo-Vázquez, D., Osborn, T. J., Castro-Díez, Y., Gámiz-Fortis, S., & Esteban-Parra, M. J. (2004). North Atlantic oscillation influence on precipitation, river flow and water resources in the Iberian Peninsula. *International Journal of Climatology*, *24*(8), 925–944. https://doi.org/10.1002/joc.1048

Turner, C. (2002). Formal status and vegetational development of the Eemian interglacial in Northwestern and Southwestern Europe. *Quaternary Research*, *58*(1), 41–44. https://doi.org/10.1006/qres.2002.2365

Turner, C., & West, R. G. (1968). The subdivision and zonation of interglacial periods. *E& G Quaternary Science Journal*, *19*(1), 93–101. https://doi.org/10.3285/eg.19.1.06

Turon, J.-L. (1984). Direct land/sea correlations in the last interglacial complex. *Nature*, *309*(5970), 673–676. https://doi.org/10.1038/309673a0

Tzedakis, P. C., Andrieu, V., de Beaulieu, J.-L., Birks, H. J. B., Crowhurst, S., Follieri, M., et al. (2001). Establishing a terrestrial chronological framework as a basis for biostratigraphical comparisons. *Quaternary Science Reviews*, *20*(16–17), 1583–1592. https://doi.org/10.1016/S0277-3791(01)00025-7

Tzedakis, P. C., Drysdale, R. N., Margari, V., Skinner, L. C., Menviel, L., Rhodes, R. H., et al. (2018). Enhanced climate instability in the North Atlantic and southern Europe during the Last Interglacial. *Nature Communications*, *9*(1), 4235. https://doi.org/10.1038/s41467-018-06683-3

Tzedakis, P. C., Hooghiemstra, H., & Pälike, H. (2006). The last 1.35 million years at Tenaghi Philippon: Revised chronostratigraphy and long-term vegetation trends. *Quaternary Science Reviews*, *25*(23–24), 3416–3430. https://doi.org/10.1016/j.quascirev.2006.09.002

Tzedakis, P. C., Pälike, H., Roucoux, K. H., & de Abreu, L. (2009). Atmospheric methane, southern European vegetation and low-mid latitude links on orbital and millennial timescales. *Earth and Planetary Science Letters*, *277*(3–4), 307–317. https://doi.org/10.1016/j.epsl.2008.10.027

Tzedakis, P. C., Raynaud, D., McManus, J. F., Berger, A., Brovkin, V., & Kiefer, T. (2009). Interglacial diversity. *Nature Geoscience*, *2*(11), 751–755. https://doi.org/10.1038/ngeo660

Tzedakis, P. C., Roucoux, K. H., de Abreu, L., & Shackleton, N. J. (2004). The duration of forest stages in southern Europe and interglacial climate variability. *Science*, *306*(5705), 2231–2235. https://doi.org/10.1126/science.1102398

Tzedakis, P. C., Wolff, E. W., Skinner, L. C., Brovkin, V., Hodell, D. A., McManus, J. F., & Raynaud, D. (2012). Can we predict the duration of an interglacial? *Climate of the Past*, *8*(5), 1473–1485. https://doi.org/10.5194/cp-8-1473-2012

Waelbroeck, C., Labeyrie, L., Michel, E., Duplessy, J. C., McManus, J. F., Lambeck, K., et al. (2002). Sea-level and deep water temperature changes derived from benthic foraminifera isotopic records. *Quaternary Science Reviews*, *21*(1–3), 295–305. https://doi.org/10.1016/S0277-3791(01)00101-9

Wagner, B., Vogel, H., Francke, A., Friedrich, T., Donders, T., Lacey, J. H., et al. (2019). Mediterranean winter rainfall in phase with African monsoons during the past 1.36 million years. *Nature*, *573*(7773), 256–260. https://doi.org/10.1038/s41586-019-1529-0

Walter, K., & Graf, H.-F. (2002). On the changing nature of the regional connection between the North Atlantic Oscillation and sea surface temperature. *Journal of Geophysical Research*, *107*(D17). ACL 7-1–ACL 7-13. https://doi.org/10.1029/2001jd000850

Williams, C., Flower, B. P., Hastings, D. W., Guilderson, T. P., Quinn, K. A., & Goddard, E. A. (2010). Deglacial abrupt climate change in the Atlantic Warm Pool: A Gulf of Mexico perspective. *Paleoceanography*, *25*(4), PA4221. https://doi.org/10.1029/2010PA001928

Yin, Q. Z., & Berger, A. (2012). Individual contribution of insolation and CO_2 to the interglacial climates of the past 800,000 years. *Climate Dynamics*, *38*(3–4), 709–724. https://doi.org/10.1007/s00382-011-1013-5

Yin, Q. Z., & Berger, A. (2015). Interglacial analogues of the Holocene and its natural near future. *Quaternary Science Reviews*, *120*, 28–46. https://doi.org/10.1016/j.quascirev.2015.04.008

Zhuravleva, A., Bauch, H. A., & Van Nieuwenhove, N. (2017). Last Interglacial (MIS5e) hydrographic shifts linked to meltwater discharges from the East Greenland margin. *Quaternary Science Reviews*, *164*, 95–109. https://doi.org/10.1016/j.quascirev.2017.03.026

Zorzi, C., Desprat, S., Clément, C., Thirumalai, K., Oliviera, D., Anupama, K., et al. (2022). When eastern India oscillated between desert versus savannah-dominated vegetation. *Geophysical Research Letters*, *49*(16), e2022GL099417. https://doi.org/10.1029/2022GL099417